# JCMM

# Journal of Computers, Mechanical and Management

e-ISSN: 3009-075X

Volume 3, Issue 1

2024

AAN PUBLISHING

Journal of Computers, Mechanical and Management
Journal homepage: www.jcmm.co.in
e-ISSN: 3009-075X
AAN PUBLISHING

# Editorial Comments: JCMM Volume 3 Issue 1

Nanjangud Subbaro Mohan*[1] and Manjunath K Vanahalli†[2]

[1]Journal of Computers, Mechanical and Management, AAN Publishing, Kangar Perlis, Malaysia 01000
[2]Department of Data Science and Intelligent Systems, Indian Institute of Information Technology, Dharwad, Karnataka, India

---

This issue of the *Journal of Computers, Mechanical and Management* (JCMM) encompasses a selection of research articles across a range of disciplines, including advanced machining methods, sentiment analysis, and the effects of macroeconomic factors on stock prices. Each study presents new perspectives and empirical findings that advance the understanding in these diverse fields.

The article by Bhat, Tandon [1], and Ahmad explores the optimization of parameters in Abrasive Water Jet Machining (AWJM) for 316 stainless steel. By examining the effects of traverse speed, standoff distance, and abrasive flow rate, the study demonstrates how these parameters influence surface roughness. Employing the Taguchi method and analysis of variance, the authors establish a regression model to predict optimal machining conditions, offering valuable insights for industrial applications in manufacturing stainless steel components.

Ahmed Shetu [2] provides a comprehensive review of non-destructive testing (NDT) techniques for aerospace composite materials, crucial for ensuring structural integrity and safety. The study examines methods like ultrasonic testing, infrared thermography, and eddy current testing, discussing their advantages, limitations, and practical applications. This work highlights future directions for integrating machine learning into NDT processes, underscoring its potential to enhance diagnostic precision and reduce inspection time.

Kulkarni and Kulkarni [3] delve into probability sampling through an experimental study on calculating the value of $\pi$ using the Monte Carlo simulation method. Their work employs non-parametric tests, including the Chi-Square and Friedman's test, to evaluate the randomness and distribution of simulation results. This research contributes to the field of mathematical simulations by showcasing practical applications of probability theory in estimating irrational numbers [3].

The study by Malhotra and Sethi [4] conducts sentiment analysis on Twitter data using supervised machine learning algorithms. The authors implement models such as Naïve Bayes, Decision Trees, and Support Vector Machines to classify tweets into positive, neutral, or negative sentiments. Their findings indicate that Support Vector Machines achieve the highest accuracy, offering insights for organizations looking to leverage social media sentiment for decision-making.

Nagvekar et al. [5] analyze the impact of inflation, bond yield rates, and the VIX index on the stock prices of Indian banks across different market capitalizations. Through regression analysis, they demonstrate how macroeconomic variables affect banks of varying sizes differently, with small-cap banks exhibiting the most sensitivity to inflation. This study offers valuable guidance for investors and policymakers by highlighting the interplay between economic indicators and banking stock performance.

This issue reflects the journal's commitment to publishing impactful research that spans a range of topics, from engineering and mathematics to data analysis and finance. Each article not only advances theoretical knowledge but also provides practical implications for industry and academia alike.

*Editor-in-Chief: editor@jcmm.co.in
†Editor:journalmanager@jcmm.co.in

**Published:** 16 October 2024

**DOI:** 10.57159/jcmm.3.1.24176.

# References


[1] Bhat, R., Tandon, V., & Ahmad, S. A. (2024). Optimizing Abrasive Water Jet Machining for Enhanced Machining of 316 Stainless Steel. *Journal of Computers, Mechanical and Management*, *3*(1). doi:10.57159/gadl.jcmm.3.1.24066.

[2] Ahmed Shetu, M. S. (2024). A Review of Nondestructive Testing Methods for Aerospace Composite Materials. *Journal of Computers, Mechanical and Management*, *3*(1). doi:10.57159/gadl.jcmm.3.1.240117.

[3] Kulkarni, S., & Kulkarni, S. (2024). The Study of the Value of $\pi$ Probability Sampling by Testing Hypothesis and Experimentally. *Journal of Computers, Mechanical and Management*, *3*(1). doi:10.57159/gadl.jcmm.3.1.240101.

[4] Malhotra, A., & Sethi, N. (2024). Conceding Sentiment Prognosis on Twitter Data. *Journal of Computers, Mechanical and Management*, *3*(1). doi:10.57159/gadl.jcmm.3.1.240105.

[5] Nagvekar, A., Kamath, R. C., Simha, T., Hegde, Y., & Prabhu, A. (2024). Analyzing the Impact of Macroeconomic Indicators on Indian Bank Stock Prices: A Quantitative Study from 2018 to 2023. *Journal of Computers, Mechanical and Management*, *3*(1). doi:10.57159/gadl.jcmm.3.1.240103.

Journal of Computers, Mechanical and Management
Journal homepage: www.jcmm.co.in
e-ISSN: 3009-075X
AAN PUBLISHING

Volume 3 Issue 1

**Article Number:** 24066

# Optimizing Abrasive Water Jet Machining for Enhanced Machining of 316 Stainless Steel

Ritesh Bhat *[1], Vipin Tandon[2], and Syed Azuan Syed Ahmad[3]

[1]Department of Mechatronics Engineering, Rajalakshmi Engineering College, Thandalam, Tamil Nadu, 602105
[2]Center of Suistainable Built Environment, Manipal School of Architecture and Planning, Manipal Academy of Higher Education, Manipal, India 576104
[3]AAN Research Center, Malaysia

**Abstract**

Abrasive Water Jet Machining (AWJM) is a non-traditional machining process renowned for its versatility and ability to cut a wide range of materials precisely. This research article presents an in-depth analysis of the optimization of AWJM parameters for machining 316 stainless steel, aiming to enhance surface quality and machining efficiency. Through a comprehensive experimental setup, the study explores the effects of varying the speed, standoff distance (SOD), and flow rate on the surface roughness (Ra) of the machined workpiece. The Taguchi method's L9 orthogonal array is employed to design the experiments, and a signal-to-noise (S/N) ratio analysis, alongside an analysis of variance (ANOVA), is utilized to discern the most significant machining parameters. Response tables for S/N ratios and means are created to summarize the effects, and main effects plots are generated to visualize trends in the data. Furthermore, a regression model is developed to correlate the machining parameters with the surface roughness, which is validated by a high coefficient of determination. Residual plots and diagnostics for unusual observations are utilized to ensure the robustness of the model. The study concludes that SOD is the most influential parameter, followed by speed and flow rate. The optimization results provide a quantitative understanding that can significantly contribute to the industrial application of AWJM for 316 stainless steel, ensuring optimal surface integrity and operational cost-effectiveness. The findings of this research offer pivotal insights for manufacturing industries that seek to integrate AWJM into their production processes.

**Keywords:** Abrasive Water Jet Machining, Surface Roughness, Optimization, 316 Stainless Steel, Taguchi Method

## 1 Introduction

Stainless steel 316 is a material known for its excellent corrosion resistance and robust mechanical properties, making it indispensable in sectors that demand high durability and resilience, such as marine engineering, biomedical devices, and chemical processing equipment [1, 2]. Despite its widespread use, machining stainless steel 316 can be challenging due to its high work hardening rate and considerable toughness, often resulting in accelerated tool wear and poor surface quality [3–5]. These challenges necessitate the exploration of non-conventional machining techniques that can mitigate the limitations posed by traditional machining. Abrasive Water Jet Machining (AWJM) has emerged as a potent solution, offering a non-contact and versatile cutting process that circumvents the thermal and mechanical stresses typically associated with conventional machining methods [6].

*Corresponding author: riteshbhat.rb@rajalakshmi.edu.in
**Received:** 06 July 2023; **Revised:** 24 November 2023; **Accepted:** 04 December 2023; **Published:** 28 February 2024

**DOI:** 10.57159/gadl.jcmm.3.1.24066.

Table 1: Chemical composition of Stainless Steel 316.

| Element | Composition (%) |
|---|---|
| Iron (Fe) | Balance |
| Chromium (Cr) | 16.0 - 18.0 |
| Nickel (Ni) | 10.0 - 14.0 |
| Molybdenum (Mo) | 2.0 - 3.0 |
| Manganese (Mn) | <2.0 |
| Silicon (Si) | <1.0 |
| Carbon (C) | <0.08 |
| Phosphorus (P) | <0.045 |
| Sulfur (S) | <0.03 |

The core mechanism of AWJM involves a high-pressure jet of water mixed with abrasive particles directed at the workpiece to effect material removal through erosion. This technique is particularly beneficial for cutting intricate shapes and handling tough materials like stainless steel 316, as it eliminates thermal distortion and reduces tool wear, while improving surface quality of the machined surface [7–9]. However, to fully exploit the capabilities of AWJM, it is crucial to optimize the machining parameters, such as jet speed, standoff distance (SOD), and abrasive flow rate, to achieve the desired surface integrity and dimensional accuracy. The complexity of the interactions between these parameters and their effects on the machining outcomes necessitates a systematic approach to their study and optimization [10]. Extensive research has been conducted in recent times to explore the effects of AWJM parameters on the surface quality and machining efficiency of various steel. For instance, Singh et al. [11] conducted a study to optimize process parameters for machining marine grade Inconel using abrasive water jet machining (AWJM) to improve surface properties and productivity. They applied Taguchi-based Grey analysis to optimize parameters for minimum surface roughness and higher material removal rate (MRR, identifying standoff distance (SOD), abrasive flow rate (AFR), and jet traverse speed (JTS) as the most influential parameters. Machining at specific values of SOD, AFR, and JTS resulted in maximum MRR and minimum surface roughness, with SOD being identified as the most significant parameter. Gawade and Jatti's [12] study focused on optimizing process parameters for minimizing taper angle in abrasive water jet machining of 304 stainless steel. They used response surface methodology, design of experiments, and ANOVA to determine the optimal parameters (traverse rate, abrasive flow rate, stand-off distance) leading to a high desirability model (0.9195) with validation results showing low percentage error (<6%) for taper angle. Rammohan's [13]study on AWJ machining of armour steel highlights that higher traverse speed and water jet pressure lead to wider kerf width and higher material removal rate. The research emphasizes the importance of these parameters for achieving optimal machining results, especially in terms of surface finish and material removal rate.

While the literature provides a solid foundation for understanding AWJM processes, there remains a need for targeted research that addresses the specific characteristics of stainless steel 316. This study aims to fill this gap by optimizing AWJM parameters to improve surface roughness and overall machining performance for this material. The study's objectives are to identify the most influential AWJM parameters on the surface roughness of stainless steel 316 and to develop a comprehensive regression model that can predict surface quality based on these parameters. The subsequent sections of this paper detail the methodology adopted for the experimental design, present the results of the machining trials and discuss the implications of the findings in the context of the existing literature. By doing so, the study contributes a nuanced understanding of AWJM parameter optimization for stainless steel 316, with the potential to inform industrial practices and future research in this domain.

# 2 Materials and Methods

## 2.1 Materials

The study employed Stainless Steel 316 (SS316), an austenitic alloy celebrated for its excellent corrosion resistance, high tensile strength, and robust mechanical properties across a wide temperature range. The choice of SS316 was driven by its prevalent use in demanding environments such as marine, chemical processing, and pharmaceutical sectors. The alloy's composition includes iron, chromium, nickel, and molybdenum, offering superior corrosion and oxidation resistance. The specific chemical composition sourced from the supplier is detailed in Table 1 to ensure reproducibility and relevance in industrial applications.

## 2.2 Equipment Setup

The experimental setup was centered around a high-precision AWJM system. This system comprised a high-power pump (37 kW) designed to generate a pressurized water stream mixed with abrasive particles directed through a precision-engineered nozzle. A CNC controller augmented the machine's cutting capabilities, ensuring meticulous control over the machining process. Key specifications include a working table dimension and a high-capacity abrasive feeder, facilitating continuous operation. The selection of SS316 as the workpiece material further underscores the study's industrial

relevance.

### 2.3 Experimental Design Using L9 Orthogonal Array

Adopting the Taguchi L9 orthogonal array, the experimental design was structured to analyze the effects of three pivotal AWJM parameters: traverse speed, stand-off distance, and abrasive flow rate. This design choice allowed for a comprehensive investigation with minimal experimental runs, focusing on efficiency and effectiveness. The parameters were chosen based on an extensive literature review and preliminary experiments to bridge the gap between theoretical knowledge and practical application.

### 2.4 Surface Roughness Measurement

The quantification of surface roughness, a critical quality attribute in machining, was meticulously conducted using a Surtronic 3+ profilometer. This instrument, known for its precision, measures the texture of machined surfaces through a diamond-tipped stylus. The procedure involved multiple measurements across different surface areas to ensure accuracy and reproducibility. Based on these measurements, the calculation of Ra values provides a reliable metric for assessing the machining process's impact on surface integrity.

Table 2: L9 Orthogonal Array for AWJM Parameters

| Experiment No. | Speed [mm/min] | SOD [mm] | Flow rate [g/min] |
|---|---|---|---|
| 1 | 30 | 2 | 200 |
| 2 | 30 | 5 | 500 |
| 3 | 30 | 8 | 800 |
| 4 | 50 | 2 | 500 |
| 5 | 50 | 5 | 800 |
| 6 | 50 | 8 | 200 |
| 7 | 70 | 2 | 800 |
| 8 | 70 | 5 | 200 |
| 9 | 70 | 8 | 500 |

## 3 Results

### 3.1 Influence of AWJM Parameters on Surface Roughness

The experimental data obtained from the Taguchi L9 orthogonal array are presented in Table 3, which showcases the interplay between the abrasive water jet machining parameters and the resultant surface roughness (Ra) of the machined 316 stainless steel samples.

Table 3: Experimental Results for AWJM on 316 Stainless Steel

| Speed (mm/min) | SOD (mm) | Flow rate (g/min) | Ra ($\mu m$) |
|---|---|---|---|
| 30 | 2 | 200 | 1.8 |
| 30 | 5 | 500 | 2.1 |
| 30 | 8 | 800 | 2.5 |
| 50 | 2 | 500 | 2.0 |
| 50 | 5 | 800 | 2.4 |
| 50 | 8 | 200 | 3.0 |
| 70 | 2 | 800 | 1.7 |
| 70 | 5 | 200 | 2.9 |
| 70 | 8 | 500 | 3.2 |

The data elucidate the effect of traverse speed, stand-off distance (SOD), and abrasive flow rate on the surface roughness of the material. Initial observations suggest that an increase in SOD and abrasive flow rate tends to correlate with an increase in Ra, indicating a rougher surface finish. In contrast, higher traverse speeds appear to contribute to a finer surface finish, as the lowest Ra value was observed at the highest speed of 70 mm/min with a SOD of 2 mm and an abrasive flow rate of 800 g/min. This trend is consistent with the understanding that higher speeds reduce the interaction time between the abrasive particles and the workpiece, resulting in a smoother surface. Further statistical analysis was conducted to quantify these parameters' effects and identify optimal settings for minimal surface roughness in AWJM of 316 stainless steel.

## 3.2 Analysis of Signal-to-Noise Ratios

The Taguchi method's signal-to-noise (S/N) ratio, which adopts the "smaller-is-better" characteristic for surface roughness, is utilized to determine the robustness of the AWJM process. The main effects plot for S/N ratios (Figure 1) indicates the influence of each machining parameter on the quality characteristic. The response table for S/N ratios

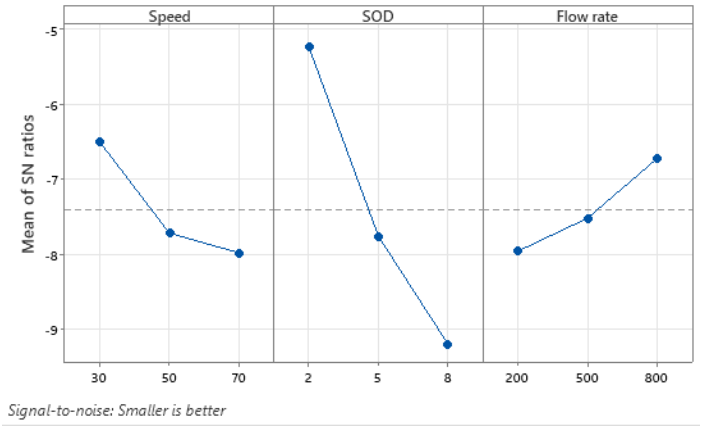


Figure 1: Main Effects Plot for S/N Ratios

Table 4: Response Table for Signal to Noise Ratios

| Level | Speed | SOD | **Flow rate** |
|---|---|---|---|
| 1 | -6.503 | -5.245 | -7.965 |
| 2 | -7.722 | -7.766 | -7.523 |
| 3 | -7.987 | -9.201 | -6.724 |
| **Delta** | 1.484 | 3.956 | 1.241 |
| **Rank** | 2 | 1 | 3 |

(Table 4) further complements the plot by quantifying the effect of each parameter level. The delta value represents the range between the highest and lowest S/N ratio for each parameter, indicating its impact on surface roughness. A higher delta signifies a more significant effect on the quality characteristic. According to the data, the SOD exhibits the highest delta value, suggesting it is the most influential parameter affecting surface roughness, followed by speed and flow rate, in that order. This preliminary analysis implies that to achieve a finer surface finish; the SOD should be carefully controlled, while the speed and flow rate can be adjusted to fine-tune the process.

## 3.3 Regression Model and Statistical Analysis

The regression model and its summary, presented in Table 5, provide a robust statistical framework for understanding the relationship between the AWJM parameters and the surface roughness of 316 stainless steel.

Table 5: Model Summary

| S | R-sq | R-sq(adj) | PRESS | R-sq(pred) | AICc | BIC |
|---|---|---|---|---|---|---|
| 0.158114 | 94.70% | 91.53% | 0.491323 | 79.18% | 17.05 | -1.96 |

The Analysis of Variance (ANOVA), detailed in Table 6, highlights the significance of the regression model. The F-values and P-values indicate that the model terms are statistically significant predictors of surface roughness.

Table 6: Analysis of Variance

| Source | DF | Seq SS | Contribution | Adj SS | Adj MS | F-Value | P-Value |
|---|---|---|---|---|---|---|---|
| Regression | 3 | 2.2350 | 94.70% | 2.2350 | 0.74500 | 29.80 | 0.001 |
| Speed | 1 | 0.3267 | 13.84% | 0.3267 | 0.32667 | 13.07 | 0.015 |
| SOD | 1 | 1.7067 | 72.32% | 1.7067 | 1.70667 | 68.27 | 0.000 |
| Flow rate | 1 | 0.2017 | 8.55% | 0.2017 | 0.20167 | 8.07 | 0.036 |
| Error | 5 | 0.1250 | 5.30% | 0.1250 | 0.02500 | | |
| Total | 8 | 2.3600 | 100.00% | | | | |

Unusual observations, potentially outliers or influential points are diagnosed with Cook's D measure, as shown in Table 7. A single observation with a high Cook's D value, observation 7, is excluded from the analysis to improve the model's accuracy.

Table 7: Fits and Diagnostics for Unusual Observations

| Observation | Ra | Fit | SE Fit | 95% CI | Resid | Std Resid | Del Resid | HI | Cook's D |
|---|---|---|---|---|---|---|---|---|---|
| 7 | 1.700 | 1.917 | 0.124 | (1.599, 2.234) | -0.217 | -2.20 | -10.61 | 0.611111 | 1.90 |

Residual plots are instrumental in verifying the assumptions of the regression analysis. As depicted in Figure 2, the normal probability plot of residuals indicates normality, and the absence of patterns in the residuals versus fits and versus order plots suggests that the residuals are randomly distributed, satisfying the assumptions of homoscedasticity and independence.

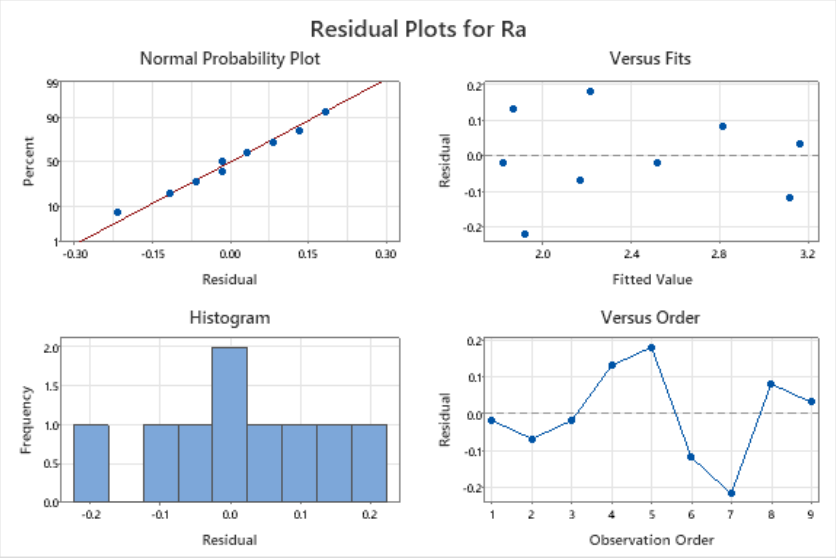


Figure 2: Residual Plots for Surface Roughness (Ra)

The regression equation, given below, encapsulates the quantitative relationship between the machining parameters and the surface finish, enabling predictions of surface roughness for given sets of parameters:

$$Ra = 1.233 + 0.0167 \times \text{Speed} + 0.1778 \times \text{SOD} - 0.000611 \times \text{Flow rate} \quad (1)$$

This equation, derived from the regression analysis, serves as a predictive model for determining the expected surface roughness (Ra) for a given combination of AWJM parameters, facilitating the optimization of the machining process.

# 4 Discussion

The optimization of AWJM parameters for the machining of 316 stainless steel is a complex interplay of process variables that directly influence the surface roughness of the finished workpiece. The experimental data indicate that both the speed of the abrasive water jet and the standoff distance (SOD) significantly affect the surface quality, with the flow rate of the abrasive mixture playing a lesser yet notable role. The physics underlying the AWJM process involves the conversion of pressure energy into kinetic energy as the water and abrasive mixture exits the nozzle. The abrasive particles, propelled by the water jet, strike the material surface with significant force, leading to material erosion primarily by micro-cutting and deformation wear mechanisms. An increase in the traverse speed of the jet results in a reduction of interaction time between the abrasive particles and the target surface, which tends to produce a finer finish. This is corroborated by the inverse relationship between speed and surface roughness observed in the experimental data. The kinetic energy imparted to the abrasive particles is a function of the square of their velocity, as described by $\frac{1}{2}mv^2$, where $m$ is the mass of the particles and $v$ is their velocity. Hence, a higher traverse speed translates to increased kinetic energy and a greater capacity for the particles to deform and erode the workpiece material. The SOD plays a pivotal role in the quality of the machined surface. With an increased SOD, there is a notable dispersion of the jet, which leads to a decrease in the energy density as the particles spread over a larger area. This dispersion results in a reduction of the localized impact forces, hence a diminished erosion efficiency and a rougher surface texture. The experimental results, reflecting the SOD as the most significant factor, align with the principles of jet dispersion and its impact on the energy delivered to the target material. The abrasive flow rate determines the number of particles available to erode the material.

At an optimal flow rate, the balance between particle mass and velocity is maintained, allowing for maximum energy transfer to the material surface without significant interference from particle collisions or agglomeration. However, if the flow rate is too high, it can result in a crowding effect, where the particles interfere with each other, reducing the efficiency of the cutting action. This phenomenon explains the negative coefficient for the flow rate in the regression equation, suggesting that beyond a certain threshold, an increase in flow rate can adversely affect surface finish. The formation of surface roughness in AWJM is governed by the mechanics of abrasive particle impact, where each particle acts as a micro-cutting tool that chips away minute fragments of the material. The quality of the surface finish is therefore a cumulative effect of these microscopic interactions, which are influenced by the parameters discussed. It is evident from the analysis that a delicate balance between speed, SOD, and flow rate is required to achieve a surface finish that meets the stringent requirements of industries employing 316 stainless steel. Understanding the mechanics behind the AWJM process is critical for its application in industry. The ability to predict the outcome of varying parameters allows for better control and optimization of the machining process, leading to improved efficiency, reduced costs, and enhanced quality of the machined parts. The discussion presented here provides a theoretical basis for the observed effects and underscores the importance of precise control over AWJM parameters to achieve desired machining outcomes.

# 5 Conclusion

In this study, the optimization of abrasive water jet machining (AWJM) parameters for the machining of 316 stainless steel was systematically investigated to enhance surface quality. The experimental results and subsequent analysis have elucidated the significant influence of process parameters on the surface roughness of the machined specimens. The standoff distance (SOD) emerged as the most impactful factor, followed by the traverse speed of the jet, and lastly, the abrasive flow rate. These findings are in line with the underlying mechanics of AWJM, where the energy density of the abrasive particles and their interaction with the workpiece surface determine the machining quality. A higher SOD was observed to disperse the jet, reducing the energy density and leading to a rougher surface, while a higher speed reduced the surface roughness due to increased kinetic energy imparted to the abrasive particles. The flow rate's inverse relationship with surface roughness underscores the need for a balanced abrasive supply to maintain cutting efficiency. The regression model developed provides a predictive capability for determining the surface roughness for given machining parameters, offering a valuable tool for process optimization in industrial applications. Future research may explore the integration of real-time monitoring and adaptive control systems in AWJM to dynamically adjust parameters and further improve surface integrity. Additionally, the extension of this study to other materials and the investigation of other AWJM parameters could provide broader insights into the versatile nature of this machining process.

# Declaration of Competing Interests

The authors declares that they has no known competing financial interests or personal relationships that could have appeared to influence the work reported in this paper.

# Funding Declaration

This research did not receive any grants from governmental, private, or nonprofit funding bodies.

# Author Contribution

# Author Contributions

**Ritesh Bhat**: Conceptualization, Methodology, Writing - Original Draft, Writing - Review & Editing, Supervision, Project Administration; **Vipin Tandon**: Data Curation, Formal Analysis, Investigation, Visualization, Writing - Review & Editing; **Syed Azuan Syed Ahmad**: Software, Validation, Resources, Writing - Review & Editing.

# References

[1] K. Lakkam, S. M. Kerur, and A. Shirahatti, "Effect of pitting corrosion on the mechanical properties of 316 grade stainless steel," *Materials Today: Proceedings*, vol. 27, pp. 497–502, 2020.

[2] S. Thaiwatthana, X.-Y. Li, H. Dong, and T. Bell, "Mechanical and chemical properties of low temperature plasma surface alloyed 316 austenitic stainless steel," *Surface engineering*, vol. 18, no. 2, pp. 140–144, 2002.

[3] J. Nomani, A. Pramanik, T. Hilditch, and G. Littlefair, "Chip formation mechanism and machinability of wrought duplex stainless steel alloys," *The International Journal of Advanced Manufacturing Technology*, vol. 80, pp. 1127–1135, 2015.

[4] L. W. H. González, Y. S. Ahmed, D. A. C. Sosa, and R. P. Rodríguez, "Enhancing aisi d2 steel milling: Balancing surface quality and tool life," 2023.

[5] A. E.-s. Abdelaziz, A. M. A. Elkaseer, and A. E.-s. Nassef, "Tool wear and surface roughness in hard turning of stainless steel 316 using tungsten carbide tool.," *MEJ-Mansoura Engineering Journal*, vol. 40, no. 5, pp. 73–82, 2021.

[6] K. Kalita, S. Chakraborty, R. K. Ghadai, and S. Chakraborty, "Parametric optimization of non-traditional machining processes using multi-criteria decision making techniques: Literature review and future directions," *Multiscale and Multidisciplinary Modeling, Experiments and Design*, vol. 6, no. 1, pp. 1–40, 2023.

[7] H. Wang, R. Yuan, X. Zhang, P. Zai, and J. Deng, "Research progress in abrasive water jet processing technology," *Micromachines*, vol. 14, no. 8, p. 1526, 2023.

[8] A. Kale, S. Singh, N. Sateesh, and R. Subbiah, "A review on abrasive water jet machining process and its process parameters," *Materials Today: Proceedings*, vol. 26, pp. 1032–1036, 2020.

[9] R. Melentiev and F. Fang, "Recent advances and challenges of abrasive jet machining," *CIRP Journal of Manufacturing Science and technology*, vol. 22, pp. 1–20, 2018.

[10] A. Anu Kuttan, R. Rajesh, and M. Dev Anand, "Abrasive water jet machining techniques and parameters: a state of the art, open issue challenges and research directions," *Journal of the Brazilian Society of Mechanical Sciences and Engineering*, vol. 43, pp. 1–14, 2021.

[11] M. K. Singh, R. Trehan, and A. Gupta, "Application of grey approach to enhance the surface properties during awj machining of marine grade inconel," *Advances in Materials and Processing Technologies*, vol. 7, no. 3, pp. 429–445, 2021.

[12] M. K. Gawade and V. S. Jatti, "To study and optimize the effects of process parameters on taper angle of stainless steel by using abrasive water jet machining," in *Techno-Societal 2020: Proceedings of the 3rd International Conference on Advanced Technologies for Societal Applications—Volume 1*, pp. 983–993, Springer, 2021.

[13] S. Rammohan, "Investigation on the performance of abrasive waterjet machining on armor steel," 2023.

Journal of Computers, Mechanical and Management
Journal homepage: www.jcmm.co.in
e-ISSN: 3009-075X
AN PUBLISHING

Volume 3 Issue 1

**Article Number:** 240103

# Effects of Inflation, Ten-Year Bond Yield Rate, and VIX Index on the Stock Prices of Banks Across All Three Market Capitalizations in India: A Regression Analysis

Anuragh Nagvekar, Raghavendra C. Kamath*, Teja Simha, Yash Hegde, and Aruna Prabhu

Department of Mechanical and Industrial Engineering, Manipal Institute of Technology, Manipal Academy of Higher Education, Manipal, Karnataka, India 576104

**Abstract**

This study investigates the impact of critical economic factors—namely, inflation, the 10-year bond yield rate, and the VIX index—on the stock prices of banks operating across different market capitalization segments in India. Through a comprehensive regression analysis framework, this research quantifies the relationships between these economic factors and bank stock prices while accounting for potential variances across large-cap, mid-cap, and small-cap banks. Utilizing data from the past five years, this analysis not only provides a nuanced understanding of how these macroeconomic indicators influence bank stock prices but also explores the specific effects on banks of varying market capitalizations. The findings reveal that small-cap companies are predominantly influenced by internal management decisions and capital allocation, whereas the consumer price index significantly predicts and reflects stock price behavior. Conversely, the bond yield rate and VIX index show minimal impact on stock prices. This study offers valuable insights for investors, policymakers, and financial institutions, aiding in the development of informed investment strategies and risk management practices.

**Keywords:** Inflation, Ten-Year Bond Yield Rate, VIX Index, Stock Prices, Market Capitalization

## 1 Introduction

Banking stocks have traditionally offered superior returns compared to broader capital markets, a trend underscored by historical performance data [1]. However, the interaction between macroeconomic variables and bank stock prices is complex, especially in emerging economies like India. Inflation, in particular, has been shown to exert a mixed impact on bank profitability and stock returns, with studies revealing both negative and positive correlations over different time horizons [1–6]. The significance of interest rates is also well documented, with the ten-year bond yield rate influencing bank NIFTY returns and indicating that bank stocks' interest rate risk exposure is closely tied to their core capital-to-asset ratio and interest spread [3, 7]. Moreover, market volatility, as measured by the VIX Index, suggests a bidirectional relationship with bank stock prices, affecting overall market returns [8]. Accounting variables such as EPS, ROE, CAR, NIM, and NPAs, alongside bank-specific factors like size and revenue diversification, emerge as significant determinants of bank stock prices and performance in India [1, 4, 9]. Notably, the performance divide between private and public sector banks reveals the influence of ownership structure on profitability [9].

*Corresponding author: cr.kamath@manipal.edu
**Received:** 09 November 2023; **Revised:** 29 November 2023; **Accepted**: 04 December 2023; **Published:** 29 February 2024

**DOI:** 10.57159/gadl.jcmm.3.1.240103.

This backdrop of varying influences on bank stock prices underscores the need for an in-depth analysis that considers the multifaceted impact of inflation, interest rates, and market volatility across banks of different sizes and ownership structures [10–12]. The current study aims to fill this gap by providing a comprehensive analysis of these relationships, thereby contributing to the nuanced understanding of the dynamics at play within the Indian banking sector's stock valuation. The findings are poised to offer valuable insights for investors, policymakers, and the banks themselves, highlighting the critical interplay between macroeconomic indicators and bank stock performance.

# 2 Methods

This study adopts a quantitative research methodology to examine the relationship between key macroeconomic indicators and the stock prices of Indian banks, categorized into large, mid, and small-cap based on their market capitalization. The analysis focuses on three primary macroeconomic indicators: the Consumer Price Index (CPI) as a measure of inflation, the ten-year bond yield rate reflecting interest rates, and the Volatility Index (VIX) representing market volatility. The impact of these indicators on the stock prices of selected banks over a specified period is assessed through regression analysis.

## 2.1 Data Collection

The dataset comprises monthly observations of the CPI, ten-year bond yield rates, and VIX Index values, alongside the closing stock prices of a stratified sample of Indian banks. These banks are classified into large, mid, and small-cap categories, based on their market capitalization, to facilitate a comparative analysis across different bank sizes. Data were collected from official sources, including the Reserve Bank of India (RBI), Securities and Exchange Board of India (SEBI), and directly from the stock exchanges where these banks are listed. The study period spans five years, from January 2015 to December 2019, providing a comprehensive overview of the trends and potential shifts in the relationships between the variables of interest.

## 2.2 Statistical Analysis

The study employs multiple regression analysis to explore the relationship between the stock prices of banks and the selected macroeconomic indicators, as it has been proven quantitative technique for the same in a few prior studies [13–17]. The regression model is specified as follows:

$$\text{Stock Price}_{it} = \beta_0 + \beta_1 \text{CPI}_t + \beta_2 \text{Bond Yield Rate}_t + \beta_3 \text{VIX Index}_t + \varepsilon_{it}$$

where $\text{Stock Price}_{it}$ represents the closing stock price of bank $i$ at time $t$, $\text{CPI}_t$ is the Consumer Price Index at time $t$, $\text{Bond Yield Rate}_t$ is the ten-year bond yield rate at time $t$, $\text{VIX Index}_t$ is the Volatility Index at time $t$, and $\varepsilon_{it}$ is the error term.

The model includes bank-specific intercepts to account for unobserved heterogeneity among banks. The analysis is conducted separately for each bank size category to identify any differential impacts of the macroeconomic indicators on stock prices. The regression coefficients ($\beta$) measure the sensitivity of bank stock prices to changes in each macroeconomic indicator. Model diagnostics and robustness checks, including tests for multicollinearity, heteroskedasticity, and serial correlation, are performed to ensure the reliability and validity of the regression results. The $R^2$ and F-statistic are reported to assess the model's overall fit and explanatory power.

# 3 Results

The empirical analysis conducted in this study explores the intricate effects of inflation (as measured by the Consumer Price Index, CPI), ten-year bond yield rates, and market volatility (as indicated by the VIX index) on the stock prices of banks across different market capitalizations in India. The results delineate the differential impacts of these macroeconomic indicators across large-cap, mid-cap, and small-cap bank stocks, elucidated through regression analysis, $R^2$, and $F$-statistics.

## 3.1 Large-cap Bank Stocks

The analysis of large-cap bank stocks focuses on some of the biggest players in the Indian banking sector, such as HDFC Bank, ICICI Bank, SBI, Kotak Bank, and Axis Bank. This section examines the influence of the Consumer Price Index (CPI), Bond Yield Rate, and the Volatility Index (VIX) on the stock prices of these large-cap banks. The regression coefficients as shown in Table **??** is obtained from the analysis that indicate the extent to which CPI, Bond Value, and VIX Index impact the stock prices of large-cap banks.

Table 1: Regression Coefficients computed for selected mid-cap bank stocks

| Company | Intercept | CPI | Bond Yield Rate | VIX index |
|---|---|---|---|---|
| HDFC BANK | -212.65 | 13.47 | -59.32 | -9.96 |
| ICICI BANK | -1873.13 | 14.88 | 26.73 | -3.81 |
| STATE BANK OF INDIA | -1222.29 | 8.06 | 57.81 | -3.24 |
| KOTAK BANK | 85.53 | 0.565 | -105.83 | -8.11 |
| AXIS BANK | -153.91 | 4.66 | 37.11 | -7.49 |

The corresponding p-values (Table 2) provide insight into the statistical significance of these coefficients, indicating how reliably the CPI, Bond Value, and VIX Index can predict the stock prices of large-cap banks.

Table 2: p-value obtained for selected large-cap bank stocks

| Large-cap Banks | HDFC BANK | ICICI BANK | SBI | KOTAK BANK | AXIS BANK |
|---|---|---|---|---|---|
| Intercept | 0.42 | 1.05E-15 | 9.52E-12 | 0.810 | 0.530 |
| CPI | 8.20E-17 | 1.69E-27 | 9.991E-19 | 4.61E-14 | 3.918E-05 |
| Bond Value | 0.011 | 0.067 | 1.48E-05 | 0.001 | 0.081 |
| VIX Index | 4.11E-06 | 0.003 | 0.002 | 0.003 | 0.0001 |

The $R^2$ values and significance F-statistics reported in Table **??** confirm the predictive power and statistical significance of the regression models applied to large-cap bank stocks. This demonstrates the models' effectiveness in explaining the variability in stock prices based on the selected economic indicators.

Table 3: $R^2$ and F computation for selected large-cap bank stocks

| Company | Significance F | $R^2$ |
|---|---|---|
| HDFC BANK | 2.15E-17 | 0.773 |
| ICICI BANK | 2.94E-26 | 0.893 |
| STATE BANK OF INDIA | 8.66E-19 | 0.798 |
| KOTAK BANK | 1.59E-14 | 0.709 |
| AXIS BANK | 1.15E-07 | 0.475 |

The findings for large-cap banks reveal a complex interplay between stock prices and macroeconomic indicators. CPI generally shows a positive correlation, suggesting that inflation may lead to an increase in bank stock prices. The impact of the Bond Value and VIX Index varies across banks, reflecting the diverse risk profiles and investment strategies employed by large-cap banks. These results are crucial for investors and financial analysts who seek to understand the factors driving the stock prices of large-cap banks in India, offering insights into how macroeconomic changes can influence investment decisions in the banking sector.

## 3.2 Mid-cap Bank Stocks

The mid-cap segment of the banking sector exhibits a distinct pattern in the impact of macroeconomic indicators on stock prices. Our regression analysis covers selected mid-cap banks such as AU Bank, IDFC First Bank, Union Bank, Canara Bank, and Federal Bank, revealing nuanced relationships between the Consumer Price Index (CPI), Bond Yield Rate, and Volatility Index (VIX) with their stock prices. The computed regression coefficients highlight the varying degrees of influence that CPI, Bond Yield Rate, and VIX Index exert on the stock prices of mid-cap banks. Notably, the CPI demonstrates a significant impact across several banks, reinforcing the notion that inflation levels can affect bank valuations in complex ways. Table 4 showcases the regression coefficients for Mid-cap Bank Stocks.

Table 4: Regression Coefficients computed for selected mid-cap bank stocks

| Company | Intercept | CPI | Bond Yield Rate | VIX index |
|---|---|---|---|---|
| AU BANK | -1078.49 | 9.85 | 9.289 | -3.417 |
| IDFC First Bank | 13.38 | 0.235 | 0.764 | -0.614 |
| UNION Bank | 28.486 | -0.637 | 20.065 | -0.664 |
| CANARA Bank | -329.117 | 0.565 | 72.581 | -2.424 |
| FEDERAL Bank | -145.448 | 0.915 | 16.048 | -0.967 |

The p-values associated with these coefficients (Table 5) underscore the statistical significance of the CPI for all banks under consideration, particularly AU Bank and Federal Bank, suggesting a robust predictive power of inflation on their stock performances. Conversely, the Bond Yield Rate and VIX Index demonstrate varied significance levels, indicating differential sensitivity among mid-cap banks to interest rate changes and market volatility.

Table 5: p-value obtained for selected mid-cap bank stocks

| | AU BANK | IDFC First Bank | UNION Bank | CANARA Bank | FEDERAL Bank |
|---|---|---|---|---|---|
| Intercept | 2.29E-07 | 0.535 | 0.314 | 0.00069 | 6.51E-05 |
| CPI | 1.12E-17 | 0.013 | 2.29E-06 | 0.1542 | 4.60E-08 |
| Bond Yield Rate | 0.546 | 0.674 | 1.927E-11 | 6.26E-13 | 5.86E-07 |
| VIX index | 0.011 | 0.0003 | 0.0017 | 0.00051 | 0.00018 |

The $R^2$ and F-statistics shown in Table 6 further validate the regression models, indicating a significant proportion of the variance in stock prices for mid-cap banks is explained by the selected macroeconomic indicators. The high $R^2$ values for banks like AU Bank and Union Bank suggest a strong model fit, capturing the essence of how inflation, interest rates, and market volatility impact their stock valuations.

Table 6: $R^2$ and F computation for selected mid-cap bank stocks

| Company | Significance F | $R^2$ |
|---|---|---|
| AU BANK | 1.23E-16 | 0.764 |
| IDFC First Bank | 8.84E-05 | 0.329 |
| UNION Bank | 1.41E-16 | 0.763 |
| CANARA Bank | 2.00E-15 | 0.738 |
| FEDERAL Bank | 1.62E-12 | 0.662 |

The findings from the mid-cap bank stocks analysis underscore the intricate ways in which macroeconomic indicators influence bank stock prices. While inflation consistently presents a significant effect, the response to bond yield rates and market volatility varies, reflecting the diverse strategic positioning and sensitivity of mid-cap banks to economic changes.

### 3.3 Small-cap Bank Stocks

Exploring the impact of macroeconomic indicators on small-cap bank stocks reveals insights into the sensitivity of smaller banks to economic fluctuations. This analysis encompasses small-cap entities such as Karnataka Bank, South Indian Bank, DCB Bank, Karur Vysya Bank, and Dhanalaxmi Bank. The regression analysis given in Table 7 provides a detailed look at how CPI, Bond Yield Rate, and the VIX index impact the stock prices of small-cap banks. The coefficients obtained highlight the unique financial dynamics small-cap banks face in response to economic changes.

Table 7: Regression Coefficients computed for selected small-cap bank stocks

| Company | Intercept | CPI | Bond Yield Rate | VIX index |
|---|---|---|---|---|
| Karnataka Bank | -99.71 | 0.025 | 27.497 | -0.731 |
| South Indian Bank | 5.50 | -0.091 | 3.416 | -0.171 |
| DCB Bank | 474.37 | -2.637 | 15.111 | -1.948 |
| Karur Vysya Bank | -82.78 | 0.0398 | 22.766 | -0.865 |
| Dhanalaxmi Bank | 22.49 | -0.048 | 0.463 | -0.176 |

The significance of these regression coefficients, as shown in the p-values (Table 8), indicates the varying degrees of impact that inflation, bond yields, and market volatility have on small-cap banks. Some variables show a significant influence on stock prices, underscoring the importance of these economic indicators in investment and valuation models for small-cap banks.

Table 8: p-value obtained for selected small-cap bank stocks

| | Karnataka Bank | South Indian Bank | DCB Bank | Karur Vysya Bank | Dhanalaxmi Bank |
|---|---|---|---|---|---|
| Intercept | 0.032536444 | 0.4146811 | 2.81361E-08 | 0.015254564 | 4.31195E-05 |
| CPI | 0.89793315 | 0.002622226 | 2.13369E-11 | 0.778899937 | 0.027945654 |
| Bond Yield Rate | 2.26739E-09 | 1.4733E-07 | 0.017207232 | 5.67407E-11 | 0.280528574 |
| VIX index | 0.029075313 | 0.000804697 | 0.000473324 | 0.000586506 | 1.07092E-05 |

The determination coefficients ($R^2$) and the F-statistic as shown in Table 9 for these banks provide a quantitative measure of the regression model's fit and its overall explanatory power regarding the stock prices of small-cap banks.

Table 9: $R^2$ and F computation for selected small-cap bank stocks

| Company | Significance of F | $R^2$ |
|---|---|---|
| Karnataka Bank | 9.34E-11 | 0.605 |
| South Indian Bank | 6.51E-12 | 0.643 |
| DCB Bank | 2.66E-13 | 0.684 |
| Karur Vysya Bank | 1.06E-13 | 0.695 |
| Dhanalaxmi Bank | 1.27E-06 | 0.431 |

The analysis for small-cap banks demonstrates that despite their size, these institutions are significantly impacted by broader economic indicators. The CPI, Bond Yield Rate, and VIX index each play a critical role in shaping the stock performance of small-cap banks, with the variability in their effects highlighting the diverse financial environments these banks operate within. This segment's findings are crucial for investors focusing on small-cap banks, offering insights into the factors driving stock prices in this market segment.

# 4 Discussion

The analysis presented in this paper elucidates the intricate relationships between macroeconomic indicators—specifically, inflation, ten-year bond yield rates, and the VIX Index—and the stock prices of Indian banks categorized by market capitalization. The differential impact observed across large, mid, and small-cap banks sheds light on the varying sensitivities and adaptive capacities within the banking sector to macroeconomic changes. Inflation, often considered a detriment to economic stability, has shown a mixed impact on bank stocks. For large and mid-cap banks, the effect of inflation appears somewhat positive, suggesting that these institutions might leverage their diversified operations and market influence to mitigate adverse inflationary effects. This capacity to adapt could be less pronounced in small-cap banks, which might explain their varied response to inflationary pressures. The sensitivity of bank stocks to interest rate fluctuations, as evidenced by the reaction to ten-year bond yield rates, particularly among large-cap banks, highlights a crucial aspect of financial management within these institutions. The negative relationship observed suggests that higher interest rates could compress net interest margins, impacting profitability. This finding underscores the importance of robust interest rate risk management strategies in safeguarding bank profitability and stock value. Furthermore, the significant role of market volatility, indicated by the VIX Index, in influencing bank stock prices, especially among small and mid-cap banks, points to the broader market sentiment and risk perception as pivotal factors in bank valuation. During periods of heightened market uncertainty, these banks' stocks appear more susceptible to adverse impacts, reflecting the need for effective risk management practices to withstand volatility. For investors, these insights underscore the importance of considering the size of a bank and its corresponding sensitivities to macroeconomic indicators when constructing investment portfolios. A nuanced understanding of these dynamics can enhance investment strategies, potentially leading to more informed decisions that account for the economic and market conditions affecting bank stocks. From a policy perspective, the findings highlight the necessity for nuanced monetary and macroprudential policies that consider the diverse impacts of economic indicators on banks of different sizes. Tailoring policy measures to address the specific needs and vulnerabilities of the banking sector could contribute to the overall stability and growth of the financial market. In essence, the study contributes to a deeper understanding of the complex interplay between macroeconomic factors and bank stock prices in India, offering valuable perspectives for investors, the banking sector, and policymakers. It paves the way for further research that could explore additional variables and their effects on the banking sector, potentially broadening the scope of understanding of financial market dynamics.

# 5 Conclusion

This study explores the effects of inflation (via the Consumer Price Index, CPI), the 10-year bond yield rate, and market volatility (via the VIX index) on the stock prices of Indian banks across different sizes from 2018 to 2023. It reveals that inflation consistently influences bank stock prices across all sizes, though its impact varies. The relationship between bank stock prices and both interest rates and market volatility is found to be more complex, indicating different sensitivities and strategies among banks of varying sizes. The findings offer key insights for investors and financial analysts, suggesting that a deep understanding of these economic indicators' impacts on banks can enhance investment decisions and risk management. Furthermore, this research contributes to the broader dialogue on financial market dynamics, encouraging further exploration into the factors affecting the banking sector. In summary, the study underscores the importance of macroeconomic indicators in shaping the stock prices of banks in India, providing valuable guidance for investors, policymakers, and the banking industry towards more robust financial strategies and policies.

## Declaration of Competing Interests

The authors declares that they have no known competing financial interests or personal relationships that could have appeared to influence the work reported in this paper.


## Funding Declaration

This research did not receive any grants from governmental, private, or nonprofit funding bodies.


## Author Contributions

**Anuragh Nagvekar**: Conceptualization, Methodology, Software, Writing - Original Draft; **Raghavendra C. Kamath** Supervision, Project Administration, Writing - Review & Editing; **Teja Simha**: Software, Validation, Investigation, Writing - Review & Editing; **Yash Hegde**: Data Curation, Formal Analysis, Visualization, Writing - Review & Editing; **Aruna Prabhu**: Supervision, Methodology, Writing - Review & Editing.

## References


[1] S. Sharma, I. Bhardwaj, and K. Kishore, "Capturing the impact of accounting and regulatory variables on stock prices of banks – an empirical study of indian banks in panel data modeling," *Asian Journal of Accounting Research*, vol. 8, no. 2, p. 184 – 193, 2023.

[2] H. Cetin, "Inflation and bank profitability: G20 countries banks panel data analysis," p. 168 – 172, 2019.

[3] Y. Chhikara and P. Desai, "Regression analysis on macroeconomic factors and dividend yield on bank nifty index returns," *Lecture Notes in Networks and Systems*, vol. 166, p. 419 – 427, 2021.

[4] C. Chandrasekhar, "Off-target on monetary policy," *Economic and Political Weekly*, vol. 49, no. 9, p. 27 – 30, 2014.

[5] Tabassum and S. Pande, "Sensitivity of non-performing assets to gdp and inflation rate volatility," *Indian Journal of Finance*, vol. 15, no. 4, p. 41 – 58, 2021.

[6] S. Chakravarty and A. Mitra, "Stock prices and inflation: Relationship revisited," *World Journal of Modelling and Simulation*, vol. 9, no. 3, p. 201 – 215, 2013.

[7] G. Banerjee, A. Das, K. Jana, and S. Shetty, "Effects of derivatives usage and financial statement items on capital market risk measures of bank stocks: evidence from india," *Journal of Economics and Finance*, vol. 41, no. 3, p. 487 – 504, 2017.

[8] B. Subburayan, "Causality and volatility spillovers of banks' stock price returns on bse bankex returns," *Journal of Corporate Accounting and Finance*, vol. 35, no. 1, p. 59 – 75, 2024.

[9] N. Gupta and J. Mahakud, "Ownership, bank size, capitalization and bank performance: Evidence from india," *Cogent Economics and Finance*, vol. 8, no. 1, 2020.

[10] J. M. Kihuro, *Interest Rate Spread, Credit Risk, Bank Size, Ownership and Financial Performance of Commercial Banks in Kenya*. PhD thesis, University of Nairobi, 2023.

[11] W. Tai, "Impact of corporate governance structures on firm performance in china," *Journal of Strategic Management*, vol. 9, no. 1, pp. 51–62, 2024.

[12] X. Wang, "Impact of macroeconomics variables on stock market indices during the period 2010-2020," *Highlights in Business, Economics and Management*, vol. 24, pp. 366–375, 2024.

[13] N. S. Ruzgar and C. Chua-Chow, "Behavior of banks' stock market prices during long-term crises," *International Journal of Financial Studies*, vol. 11, no. 1, 2023.

[14] H. Rjoub, I. Civcir, and N. G. Resatoglu, "Micro and macroeconomic determinants of stock prices: The case of turkish banking sector," *Romanian Journal of Economic Forecasting*, vol. 20, no. 1, p. 150 – 166, 2017.

[15] N. P. Ha, "Impact of macroeconomic factors and interaction with institutional performance on vietnamese bank share prices," *Banks and Bank Systems*, vol. 16, no. 1, p. 127 – 137, 2021.

[16] A. K. Mallick, A. K. Mishra, and I. Vyas, "Forecasting stock prices of five major commercial banks in india and stress testing: A multivariate approach," *Journal of Public Affairs*, vol. 21, no. 3, 2021.

[17] M. Al-Dwiry, G. N. Al-Eitan, and W. Amira, "Factors affecting stock price: Evidence from commercial banks in the developing market," *Journal of Governance and Regulation*, vol. 11, no. 4 Special Issue, p. 339 – 346, 2022.

Journal of Computers, Mechanical and Management
Journal homepage: www.jcmm.co.in
e-ISSN: 3009-075X
AN PUBLISHING

Volume 3 Issue 1

**Article Number:** 240105

# Conceding Sentiment Prognosis on Twitter Data

Anshu Malhotra*[1] and Nishu Sethi[2]

[1]Department of Applied Sciences, The NorthCap University, Gurugram, India 122017
[2]Department of Computer Science and Engineering, School of Engineering, The NorthCap University, Gurugram, Haryana, India 122017

**Abstract**

Twitter is the biggest micro-blogging website that gives people a platform to share their opinions about any new happenings around the world. The size of tweets is generally short, which makes it very suitable for opinion mining. The key focus of the paper is to analyze the feelings and ideas. In this paper, analysis is done on the classification of tweets on a particular keyword. The tweets related to the given keyword are collected, analyzed, and the result is generated in the form of percentage of positive, neutral, and negative sentiments, which gives us a sense of the overall sentiment of the keyword. Further, Classification is done using supervised learning algorithms and the best among these will be found by calculating the accuracy of each.

**Keywords:** Sentiment Analysis, Logistic Regression, Support Vector Machines Opinion Mining, Supervised Machine Learning, Naïve Bayes, Decision Tress, Accuracy, Polarity Prediction.

## 1 Introduction

The classification of data is a continuously emerging topic among data scientists due to the continuously growing demand for classification. The main reason being that it allows analyzing the data globally, which can be used to derive a lot of information. The type of classification being discussed here is the classification of text. Text classification into already defined classes is also known as sentiment analysis [1], which recognizes the emotional aspect of the given content and assigns meaning to the sentiment, e.g., neutral, negative, and positive. Sentiment analysis [2] can be used in almost every aspect of the modern world, from products to services, e.g., online marketing, healthcare, social media. It can also be used in financial services or in political areas, and other possible domains where people leave their opinion. Organizations look to collect public or consumer opinions about their services and products. For that, opinion gathering methods such as surveys are conducted with the focus on targeted groups. So, modern solutions like sentiment analysis that work on topics such as classification using machine learning algorithms and work with collections of people's feedback or data expressed within short text messages, e.g., tweets, reviews of products prove to be very helpful. The results of this paper can be used in a variety of largescale data processing systems, finding the optimal information and their values to implement the algorithms, understanding and predicting the data to support decision making, and for knowledge gathering process. In this paper, Support Vector Machines, Naïve Bayes, Decision Tree, and Logistic Regression classifiers [3] are used for the classification task to get percentage-wise classification of sentiment on the keyword and to get the best classification accuracy using a number of tweets from Twitter. These methods are the most accurate and popular classification methods in the given domain of research.

*Corresponding author: anshumalhotra@ncuindia.edu
**Received:** 14 November 2023; **Revised:** 29 November 2023; **Accepted**: 04 December 2023; **Published:** 29 February 2024

**DOI:** 10.57159/gadl.jcmm.3.1.240105.

## 2 Methods

Sentiment Analysis is performed using Twitter APIs. With the help of these four keys, viz., Consumer Key, Consumer Secret, Access Token, and Access Token Secret, Twitter can be accessed. Tweedy is an open-source and easy-to-use library that allows access to the Twitter API [4]. The Tweets can now be fetched and are stored in a JSON format. A Labelled dataset is also downloaded. Natural Language Processing (NLP) is applied to both datasets to clean the data. With classification algorithms, tweets can be classified into positive, neutral, and negative polarity. Distinct classification algorithms like Support Vector Machine (SVM), Logistic Regression (LR), Naïve Bayes (NB), and Decision Trees (DT) [5] are utilized for categorization and further, the performance for each classifier can be measured in terms of accuracy. The design to build the proposed methodology is depicted in Figure 1.

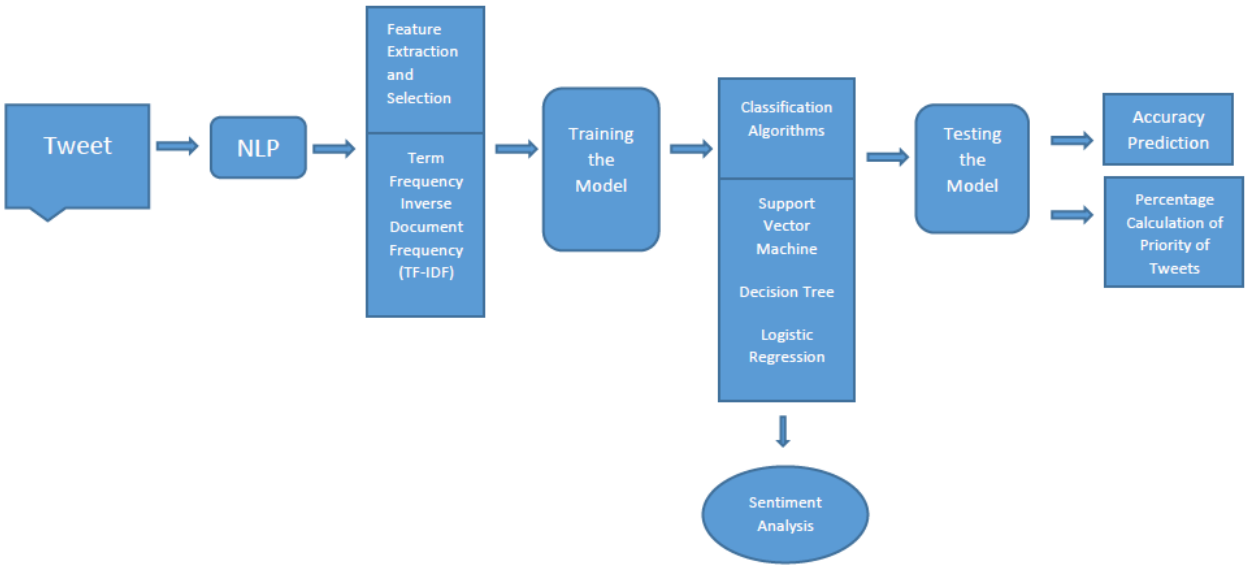


Figure 1: Workflow for the Methodology.

### 2.1 Extraction of Tweets

- **Getting Authentication Credentials**
  Authentication credentials such as Consumer Key, Consumer Secret, Access Token, and Access Token Secret can be generated by creating an application on Twitter. By visiting the Twitter Developer Website and providing all the necessary details, a Twitter Application can be created.

- **Authenticating Python Script**
  After establishing all the login credentials, that is APIs and Access Tokens, authentication can progress. To initialize authentication, some Python libraries need to be imported.

- **Defining Keywords**
  Keywords are the search words that search for tweets involving the specified keyword. Keywords are termed as input which is in the form of a string. A thousand tweets are fetched and stored in a JSON format.

### 2.2 Pre-processing the Tweets

Pre-processing is an important aspect of data mining. Pre-processing is a screening phase which means analyzing data such that the data should not result in any misleading results. This ensures quality and a good representation of data, which is extremely important to begin any analysis. In this project, Natural Language Processing (NLP) [6–8] is used by importing the Natural Language Toolkit (NLTK) library as the medium to screen and clean the data. Various techniques for processing natural language context are:

1. **Tokenization**: It is the practice of breaking a large set of contexts into smaller text or terms. Tokenization is of two types, namely Sentence Tokenization, which means breaking text into sentences, and Word Tokenization, which means splitting sentences into words.

2. **Removal of Stop Words**: Stop-words are English words that do not add meaning to a sentence and therefore can be disregarded. For example, 'have', 'the', 'are', 'was', etc.

3. **Lexicon Normalization**: It is the process of translating a non-standard text to a standard one. The goal is to eliminate various forms of words thus retaining a single and actual representation. For example, 'play', 'playing', 'playable', etc., can be reduced to "play" to retain the core meaning. Lexicon Normalization is of two types, namely:

- Stemming is the process of reducing the morphological variants of a root or base word. The aim is to remove affixes, i.e., prefixes and suffixes, for example, reducing the words “chocolates”, “chocolatey”, and “choco” to the root word “chocolate”.
- Lemmatization is the process of grouping different forms of a word so that they can be analyzed as a single item.

The workflow for pre-processing tweets is shown in Figure 2.

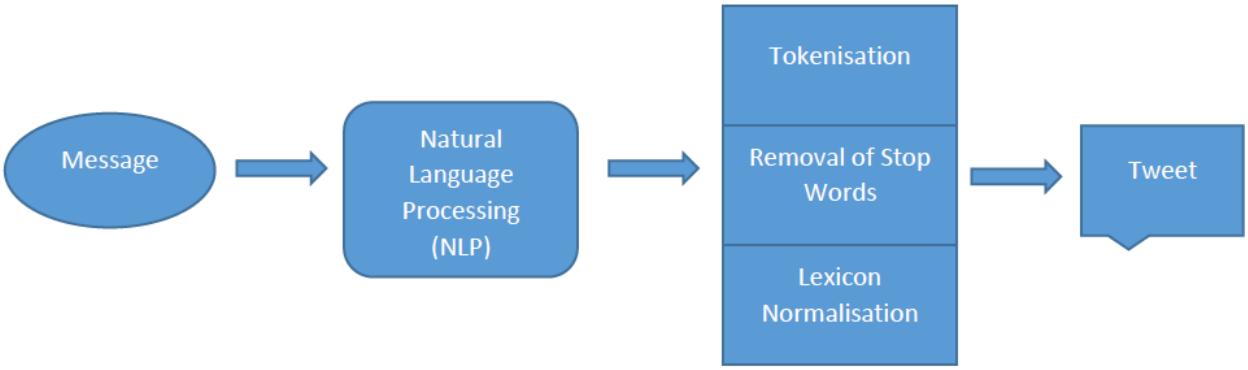


Figure 2: Workflow for Pre-processing Tweets.

## 2.3 Feature Extraction and Selection

Feature Extraction is the practice of selecting variables into features by efficiently reducing the amount of data that must be processed. Essentially, feature extraction involves extracting useful features from existing data. Conversely, Feature Selection refers to the process of filtering out irrelevant and unessential characteristics from the dataset, thereby choosing the most relevant attributes. In our project, the technique employed for extracting and selecting features is “Term Frequency–Inverse Document Frequency” (TF-IDF) [9, 10], a methodology that quantifies the importance of a term in a document. The weight assigned to each term indicates its significance within the corpus. This technique is widely utilized in the field of Knowledge Retrieval.

## 2.4 Training the Model with Machine Learning Algorithms

Supervised Learning Algorithm [11] is the machine learning task of instructing the model to learn a function that maps an input to an output based on example input-output pairs. It derives a function from a labeled training dataset that consists of a set of training examples. In supervised learning, each example is a pair consisting of an input object (vector) and a desired outcome value (supervisory signal). This kind of learning algorithm analyzes the training data and produces an inferred function, which can be used for mapping new instances. An optimal model allows the algorithm to correctly predict the class labels for unseen instances, thus applying the learned function to new data in a ”reasonable” way. The process of mapping from input to output using the supervised learning algorithm is illustrated in Figure 3.

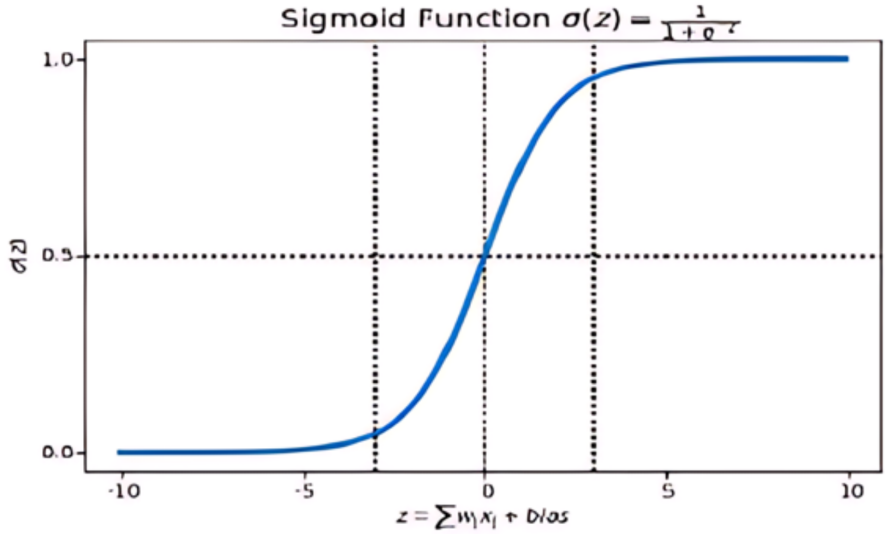


Figure 3: Illustration of the supervised learning process.

The various types of supervised learning algorithms include:

1. **Naïve Bayes (NB)**: A Classification Algorithm [12] part of a family of probabilistic algorithms based on Bayes' Theorem with a "naive" assumption of independence among each set of features. The theorem computes the probability $P(c|x)$, where $c$ is the class of the possible outcome and $x$ is the given instance to be categorized, with certain attributes. The formula used is as shown in Eq. (1)

$$P(c|x) = \frac{P(x|c) \cdot P(c)}{P(x)} \tag{1}$$

2. **Support Vector Machine (SVM)**: SVM [13] are Supervised Learning algorithms that analyze data for categorization. An SVM training algorithm builds a model that assigns new examples to one category or the other, making it a non-probabilistic binary linear classifier. The optimal hyperplane is identified such that it maximizes the margin between the two classes.

3. **Decision Trees (DT)**: The Decision Tree algorithm [14] is used in statistics, data mining, and machine learning as a predictive modeling tool. It moves from observations about an item (represented in the branches) to conclusions about the item's target value (represented in the leaves). Leaves represent class labels and branches represent conjunctions of features that lead to those class labels.

4. **Logistic Regression (LR)**: This learning algorithm [15, 16] is used for estimating the probability of a binary outcome. It is modeled by the logistic function, as represented by Eq. (2).

$$P(Y = 1|X) = \frac{1}{1 + e^{-(\beta_0 + \beta_1 X)}} \tag{2}$$

### 2.5 Testing the Model

Testing is the phase where the model, trained in the training phase, is evaluated based on its performance. In the proposed system, the testing phase consists of two components: Accuracy Prediction and Percentage Calculation of Polarity of Tweets. Further, both Accuracy Prediction and Percentage Calculation of Polarity of Tweets are graphically depicted with the help of a Pie-Chart.

## 3 Results and Discussion

This section presents the details of the experiments conducted in this project along with the discussion of the outcomes. In addition to sentiment analysis, the polarity percentage is calculated [17], with the goal of determining the accuracy [18]. Various classifiers such as Decision Trees (DT), Support Vector Machines (SVM), Naïve Bayes (NB), and Logistic Regression (LR) are employed to analyze the accuracy of each classifier. The primary reason for using four different classifiers is to compare their accuracies. A total of 1000 tweets were collected from Twitter using Twitter APIs, and 48 tweets were analyzed from the downloaded dataset after pre-processing. Sentiments such as positive, neutral, and negative are validated using both datasets, namely the Downloaded and the Extracted Dataset. The following Table 1 and Figure 4 depict the polarity calculation in terms of the number of tweets with all four classifiers used on the Extracted Dataset.

Table 1: Polarity Calculation for the extracted data with different classifiers.

| Classifier | Positive | Neutral | Negative |
|---|---|---|---|
| Naïve Bayes (NB) | 176 | 225 | 599 |
| Support Vector (SVM) | 123 | 5 | 872 |
| Decision Tree (DT) | 23 | 147 | 830 |
| Logistic (LR) | 188 | 14 | 798 |

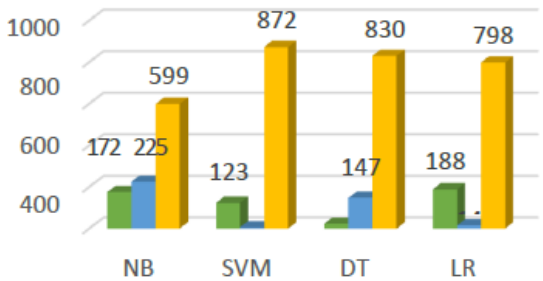


Figure 4: Graphical Representation of Tweets from Extracted Dataset.

The polarity calculation for the downloaded dataset is presented in Table 2 and the graphical representation is shown in Figure 5. This dataset was used to validate the performance of the different classifiers on a pre-existing, processed collection of data. However, after pre-processing and training the model, it was established that Logistic regression has the maximum accuracy. The following table shows the accuracy in terms of percentage of each classifier. Also, the figure depicts the graphical representation of the same. As a result, Logistic Regression shows highest accuracy.

Table 2: Polarity Calculation for the Downloaded Dataset with different classifiers..

| Classifier | Positive | Neutral | Negative |
|---|---|---|---|
| Naïve Bayes (NB) | 8 | 19 | 21 |
| Support Vector Machine (SVM) | 12 | 12 | 24 |
| Decision Trees (DT) | 9 | 17 | 22 |
| Logistic Regression (LR) | 13 | 11 | 24 |

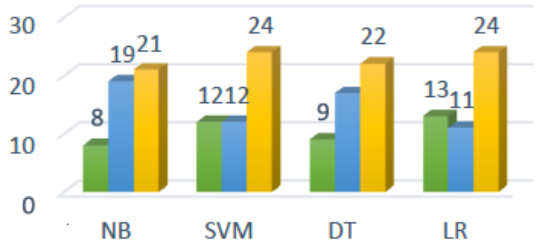


Figure 5: Graphical Representation of Tweets from Downloaded Dataset.

The analysis of the downloaded dataset allows for a direct comparison between the various machine learning algorithms in terms of their ability to classify sentiment accurately. It can be observed from Table 2 and Figure 5 that different classifiers exhibit varying levels of performance with respect to the sentiment classification task.

The accuracy of each classifier is quantified and presented in Table 3, while Figure 6 provides a visual representation of these accuracies.

Table 3: Accuracy Matrix of the classifiers.

| Classifier | Accuracy (%) |
|---|---|
| Naïve Bayes (NB) | 66.666 |
| Support Vector Machine (SVM) | 64.583 |
| Decision Tree (DT) | 39.583 |
| Logistic Regression (LR) | 69.416 |

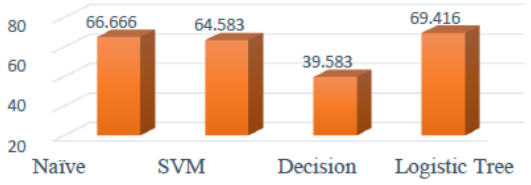


Figure 6: Graphical Representation of Accuracy Prediction.

The analysis of the accuracy of the classifiers is critical to understanding their performance. As shown in Table 3 and Figure 6, the Logistic Regression (LR) classifier achieves the highest accuracy, while the Decision Tree (DT) classifier has the lowest accuracy among the four classifiers. These results are significant in the context of sentiment analysis where the precision of prediction is paramount. The calculation of the percentage polarity of Tweets is visualized using graphical representation [19]. A Pie-Chart is drawn to depict the proportion of polarity (Negative, Positive, and Neutral) for both datasets. The accuracy with the count, i.e., the number of tweets, is also displayed in Figure 7. The graphical representation for one of the classifiers could not be shown below. The first pie-chart represents the analyzed Tweets from the Downloaded Dataset and the second pie-chart represents analyzed Tweets from the Extracted Dataset.

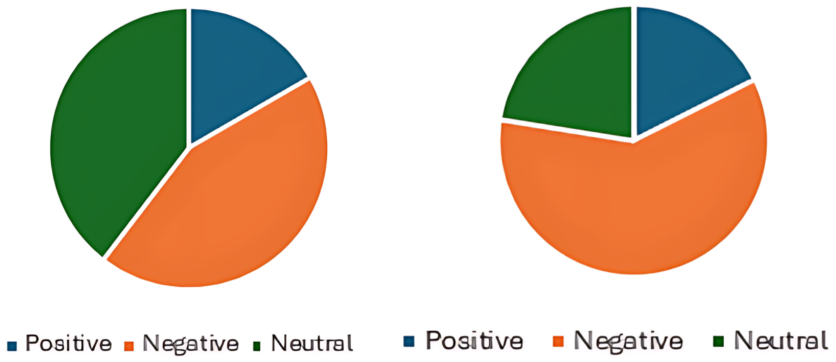


Figure 7: Graphical representation of Naïve Bayes.

# 4 Conclusions

In this paper, the sentiments of people on a particular keyword are analyzed in terms of percentage for negative, positive, and neutral sentiments, as well as the adoption of various machine learning algorithms for the classification of sentiments to determine the approach with the maximum accuracy. The data used in this study is a collection of tweets from the social media platform Twitter. Various classification models have been tested to reflect the best model in terms of accuracy. Further improvements to the models can be achieved by exploring different methodologies and expanding domain knowledge, including the implementation of emoticon analysis, understanding order dependence, and detecting sarcasm. Despite the challenges and complexities inherent in opinion analysis, its value to business and decision-making cannot be overlooked. Sentiment prediction relies on human-like aspects, suggesting that it will become a major influence in industry decisions in the foreseeable future. Enhancing the precision and reliability of extraction methods could help address some of the current challenges in sentiment prediction. Looking forward, a more refined and accurate representation of public opinion is envisioned, established through Sentiment Prediction. This vision includes a societal construct where every opinion is considered, and each sentiment contributes to decision-making processes, transcending the need to rely solely on a few 'experts'. It is towards this future that sentiment analysis endeavors to contribute significantly.

## Declaration of Competing Interests

The authors declares that they have no known competing financial interests or personal relationships that could have appeared to influence the work reported in this paper.

## Funding Declaration

This research did not receive any grants from governmental, private, or nonprofit funding bodies.

## Author Contribution

**Anshu Malhotra**: Supervision, Project Administration, Writing - Review & Editing; **Nishu Sethi** Conceptualization, Methodology, Software, Writing - Original Draft

## References

[1] L. Rajput and S. Gupta, "Sentiment analysis using latent dirichlet allocation for aspect term extraction," *Journal of Computers, Mechanical and Management*, vol. 1, no. 2, pp. 30–35, 2022.

[2] M. V. Mäntylä, D. Graziotin, and M. Kuutila, "The evolution of sentiment analysis—a review of research topics, venues, and top cited papers," *Computer Science Review*, vol. 27, pp. 16–32, 2018.

[3] M. Trupthi, S. Pabboju, and G. Narasimha, "Sentiment analysis on twitter using streaming api," in *Proceeding of IEEE 7th International Advance Computing Conference*, pp. 915–919, IEEE, 2017.

[4] G. Santafe, I. Inza, and J. A. Lozano, "Dealing with the evaluation of supervised classification algorithms," *Artificial Intelligence Review*, vol. 44, pp. 467–508, 2015.

[5] B. Wagh, J. Shinde, and P. Kale, "A twitter sentiment analysis using nltk and machine learning techniques," *International Journal of Emerging Research in Management and Technology*, vol. 6, no. 12, pp. 37–44, 2018.

[6] P. M. Nadkarni, L. Ohno-Machado, and W. W. Chapman, "Natural language processing: an introduction," *Journal of the American Medical Informatics Association*, vol. 18, no. 5, pp. 544–551, 2011.

[7] R. Egger and E. Gokce, "Natural language processing (nlp): An introduction: Making sense of textual data," in *Applied data science in tourism: Interdisciplinary approaches, methodologies, and applications*, pp. 307–334, Springer, 2022.

[8] J. Kaur, P. Verma, and S. Bajoria, "Sashakt: a job portal for women using text extraction and text summarization," *Journal of Computers, Mechanical and Management*, vol. 1, no. 2, pp. 22–29, 2022.

[9] F. Osisanwo, J. Akinsola, O. Awodele, J. Hinmikaiye, O. Olakanmi, J. Akinjobi, *et al.*, "Supervised machine learning algorithms: classification and comparison," *International Journal of Computer Trends and Technology*, vol. 48, no. 3, pp. 128–138, 2017.

[10] P. Kaviani and S. Dhotre, "Short survey on naive bayes algorithm," *International Journal of Advance Engineering and Research Development*, vol. 4, no. 11, pp. 607–611, 2017.

[11] Y. Yang, J. Li, and Y. Yang, "The research of the fast svm classifier method," in *Proceedings of 12th International Computer Conference on Wavelet Active Media Technology and Information Processing*, pp. 121–124, IEEE, 2015.

[12] N. Bhateja, N. Sethi, and S. Kaushal, "Machine learning and its role in diverse business systems," *Research Journal of Science and Technology*, vol. 13, no. 3, pp. 213–217, 2021.

[13] N. Sethi, N. Bhateja, N. Sethi, and S. Sinha, "Recognizing sentiment prediction on twitter data," *International Journal of Innovative Research in Computer Science & Technology*, pp. 2347–5552, 2020.

[14] L. Rokach and O. Maimon, "Decision trees," *Data Mining and Knowledge Discovery Handbook*, pp. 165–192, 2005.

[15] L. Liu, "Research on logistic regression algorithm of breast cancer diagnose data by machine learning," in *2018 International Conference on Robots & Intelligent System (ICRIS)*, pp. 157–160, IEEE, 2018.

[16] S. Deepa, "Metaheuristics for multi criteria test case prioritization for regression testing," *Journal of Computers, Mechanical and Management*, vol. 1, no. 1, pp. 42–51, 2022.

[17] I. Bala and A. Yadav, "Comprehensive learning gravitational search algorithm for global optimization of multimodal functions," *Neural Computing and Applications*, vol. 32, pp. 7347–7382, 2020.

[18] S. Jain, D. C. Bisht, and P. C. Mathpal, "Particle swarm optimised fuzzy method for prediction of water table elevation fluctuation," *International Journal of Data Analysis Techniques and Strategies*, vol. 10, no. 2, pp. 99–110, 2018.

[19] A. Hasan, S. Moin, A. Karim, and S. Shamshirband, "Machine learning-based sentiment analysis for twitter accounts," *Mathematical and Computational Applications*, vol. 23, no. 1, p. 11, 2018.

Journal of Computers, Mechanical and Management
Journal homepage: www.jcmm.co.in
e-ISSN: 3009-075X
AN PUBLISHING

Volume 3 Issue 1

**Article Number:** 240101

# The Study of the Value of $\pi$ Probability Sampling by Testing Hypothesis and Experimentally

Sanjay Kulkarni*[1] and Sandeep Kulkarni[2]

[1]Department of First Year Engineering, Hope Foundation's Finolex Academy of Management and Technology, Ratnagiri, Maharashtra, India, 415639
[2]Tata Consultancy Services, Pune, Maharashtra, India

**Abstract**

This study evaluated the value of $\pi$ using the Monte Carlo Simulation Method and compared the results with experimental values. The experimental value of $\pi$ was determined by considering a unit circle $|z| = 1$ centered at the origin, inscribed within a square with vertices $(0, 0)$, $(1, 0)$, $(1, 1)$, and $(0, 1)$. Points were randomly generated within the square, where points satisfying $|z| \leq 1$ lay within the circle, and those with $|z| \geq 1$ lay outside the circle but within the square. By selecting large numbers of random pairs and determining their positions relative to the circle, the ratio $\pi = \frac{4n}{N}$ was calculated, where $N$ was the total number of points and $n$ was the number of points within the circle. Larger sample sizes yielded values of $\pi$ closer to the true value. The distribution of Monte Carlo Simulation results, using 20 triplets of random numbers, was examined with non-parametric tests such as Friedman's Test. Ranks were assigned to the 20 random numbers row-wise for each triplet. The null hypothesis, asserting that all triplets had identical effects, was tested and showed significant differences at the 5% level. Additionally, the distribution was tested for goodness of fit using a Chi-Square Test at a 5% significance level. Results indicated that the triplets of random numbers conformed to the expected distribution.

**Keywords:** Random Number; Triplets; Non-Parametric Test; Friedman's Test; Chi-Square Test

## 1 Introduction

The technique of simulation is extensively utilized in the physical sciences and is increasingly becoming a crucial tool for addressing complex problems in managerial decision-making. Scale models of machines are used to simulate plant layouts, and models of aircraft are tested in wind tunnels to determine their aerodynamic characteristics. Simulation, aptly described as a management laboratory, assesses the effects of various alternative policies without disrupting the real system. Techniques such as linear programming, dynamic programming, queuing theory, and network models are insufficient to tackle all significant managerial problems requiring data analysis, each having its limitations. When characteristics such as uncertainty, complexity, dynamic interaction between decisions and subsequent events, and the need to develop detailed procedures with finely divided time intervals combine in one scenario, it becomes too complex for traditional mathematical programming and probabilistic models. Such situations necessitate analysis by alternative quantitative techniques that provide accurate and reliable results. The Monte Carlo method of simulation, developed by mathematicians John von Neumann and Stanislaw Ulam during World War II, was initially used to study neutron travel through various materials. The technique provided an approximate but workable solution to this problem and soon became popular, finding numerous applications in business and industry.

*Corresponding author: sanjay.kulkarni@famt.ac.in
**Received:** 02 September 2023; **Revised:** 16 December 2023; **Accepted**: 16 December 2023; **Published:** 29 February 2023

**DOI:** 10.57159/gadl.jcmm.3.1.240101.

It is now a vital tool in the operations researcher's toolkit [1–7]. In computer science and its applications, new or improved algorithms are compared with existing ones on several datasets to demonstrate superior performance. Let $x_1$ represent the control algorithm, and $x_2, x_3, x_4, \ldots, x_k$ represent the $k-1$ benchmark algorithms. The challenge lies in better judging whether the control algorithm $x_1$ has a significant advantage over other benchmark algorithms on experimental datasets. Due to dataset diversity and various random factors in training and testing, it is rare for the control algorithm to perform better on all datasets. Therefore, meaningful conclusions require statistical hypothesis tests [8]. These tests are categorized into parametric and non-parametric tests [9–11]. Parametric tests assume that the data follows a known probability distribution and make inferences about distribution parameters [10]. Conversely, non-parametric tests typically have no preliminary assumptions about the data distribution, making them applicable in various circumstances. Most non-parametric tests use rankings instead of raw data for hypothesis testing. A transformation procedure is adopted to obtain rankings for control and benchmark algorithms [9, 10]. The choice of statistical tests depends on the specific application, data characteristics, and researcher preferences. Parametric tests often have assumptions regarding data characteristics for comparison. For instance, analysis of variance (ANOVA) requires data to meet conditions such as independence, normality, and homogeneity [10]. When these assumptions are met, parametric tests are more effective [10]. Otherwise, parametric tests can produce biased conclusions. In practical applications, it is rarely possible to verify that algorithm results on different datasets satisfy these assumptions. Therefore, non-parametric tests are commonly considered [9, 12]. When selecting a non-parametric test, it is necessary to distinguish between pairwise and multiple comparisons. Non-parametric tests for pairwise comparisons include the Wilcoxon signed-rank test [13]. For multiple comparisons, non-parametric tests include the Friedman test, multiple sign tests [14], and contrast estimation based on medians [15]. Although non-parametric tests are widely adopted in published papers [16–19], the Friedman test is particularly effective and widely used by many scholars [20, 21]. O'Gorman [22] compared the F-test, Friedman test, and several aligned Friedman tests using Monte Carlo simulation. The Monte Carlo technique employs random numbers and is suitable for problems involving probability where physical experimentation is impractical, and mathematical model formation is impossible. It is a simulation method using a sampling technique. The steps involved in conducting a Monte Carlo simulation are:

- Select the measure of effectiveness of the problem.
- Identify the variables that significantly affect the measure of effectiveness.
- Determine the cumulative probability distribution of each variable selected in step 2.
- Generate a set of random numbers.
- Consider each random number as a decimal value of the cumulative probability distribution.
- Record the value(s) of the variables generated in step 5. Substitute in the formula chosen for the measure of effectiveness and find its simulated value.
- Repeat steps 5 and 6 until the sample is large enough to satisfy the decision maker.

This paper aims to study the value of $\pi$ obtained through the Monte Carlo Simulation method and to compare the results with experimental values. The Monte Carlo Simulation distribution is tested by applying non-parametric hypothesis testing methods, such as Friedman's Test and the Chi-Square Test.

# 2 Methods

## 2.1 Experimental Determination of $\pi$

The coordinate axes $OX$ and $OY$ were drawn. With center $O$, an arc $PR$ of unit radius was drawn, completing the square $OPQR$ as shown in Figure 1. The equation of the circle was established as $x^2+y^2=1$. From the random number table, two numbers were selected, specifically 0.2068 and 0.7295, and were assigned as values to $x$ and $y$ respectively. The point $P_1(0.2068, 0.7295)$ was plotted. If $x^2+y^2 \leq 1$, then $P_1$ lay inside or on the arc of the circle. Conversely, if $x^2+y^2>1$, $P_1$ lay outside the arc but within the square.

Several pairs of random numbers were continuously selected, and it was determined whether the points represented by these numbers fell within or on the arc, or outside the arc but within the square. Let $N$ represent the total number of points considered, and $n$ represent the number of points that lay in or on the arc. Then, the Equation (1) was established:

$$\frac{n}{N} = \frac{\text{Area enclosed by the arc}}{\text{Area of the square}} \tag{1}$$

As the area enclosed by the arc is $\frac{\pi}{4}$ and the area of the square is 1, the ratio was calculated as given by Equation (2):

$$\frac{n}{N} = \frac{\pi}{4} \tag{2}$$

From this, $\pi$ was calculated using the Equation (3):

$$\pi = \frac{4n}{N} \tag{3}$$

This equation provided the experimental value of $\pi$. The method demonstrated that the larger the sample size $N$, the closer the obtained value was to the true value of $\pi$, effectively illustrating the utility of geometric random sampling for approximating $\pi$, as depicted in Figure 1.

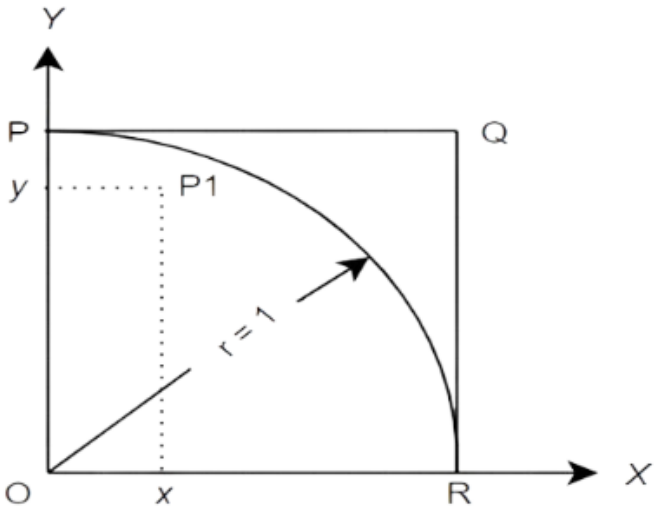


Figure 1: Illustration of points inside or outside the arc but within the square.

## 2.2 Monte Carlo Simulation Approach

Three points were chosen at random on the circumference of a circle using Monte Carlo methods to determine the probability that they lie on the same semicircle. A circle of circumference unity, i.e., of radius $\frac{1}{2\pi}$, was drawn as depicted in Figure 1. A triplet of random numbers (0.48, 0.51 and 0.06) was selected from the random number table. These numbers were plotted as points A, B and C on the circumference in Figure 2, with their positions from point $O$ along the circumference measured anticlockwise. Since the difference between the maximum (0.51) and minimum (0.06) values in this triplet was less than 0.50, the points were determined to lie on the same semicircle. The following general rule was applied to ascertain whether a triplet of random numbers lies on a semicircle:

1. The difference between the maxima and minima needs to be calculated. If this difference is $\leq 0.50$, the triplet is considered to lie on a semicircle.

2. If the difference is $> 0.50$, unity is added to those random numbers in the triplet that were $< 0.50$ and to the minimum random number in the triplet. The new difference between the maxima and minima needs to be then found. If this difference is $\leq 0.50$, the triplet is considered to lie on a semicircle; otherwise, it did not.

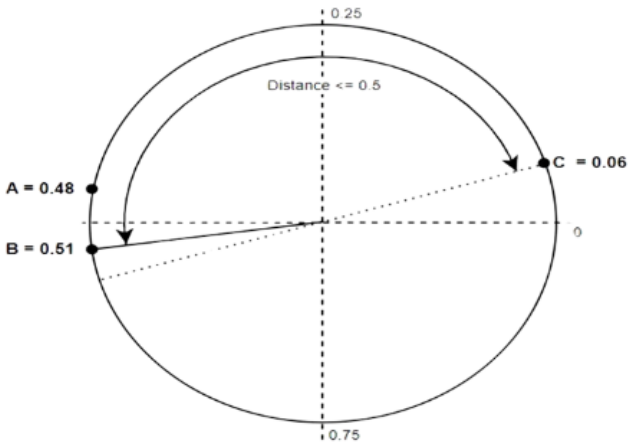


Figure 2: Three points chosen at random on the circumference of a circle using Monte Carlo methods.

### 2.3 Friedman's Test / Two-Way Analysis of Variance by Ranks

Friedman's test is a non-parametric test utilized to identify differences across multiple treatments on the same subjects. Being non-parametric, this test does not assume that the data originates from a specific distribution, such as the normal distribution. This test is effectively an extension of the sign test and is applied when there are more than two treatments, although it reduces to the sign test with only two treatments. This statistic is applicable in two distinct scenarios that may seem different but fundamentally address the same statistical question: either measuring the same quantitative variable at different times or measuring different comparable quantitative variables from the same sample. In both cases, Friedman's test serves to compare the distributions of the variables and thus, it was used in the present work.

### 2.4 Chi Square ($\chi^2$) Test to Test the Goodness of Fit

The $\chi^2$ test, a non-parametric statistic, is utilized to evaluate the degree of correspondence between observed frequencies and those expected under a specified hypothesis. This test is especially appropriate for categorical data as it does not assume a normal distribution. Given these characteristics, the $\chi^2$ test is particularly well-suited for the analysis of triplet data in this study. It was thus used in the present work to provide a methodological framework to assess whether observed variances from expected frequencies were statistically significant, thereby testing the underlying hypotheses of the research.

## 3 Results

### 3.1 Monte Carlo Simulation Outcomes

Table 1 presents the results of the Monte Carlo simulation approach, indicating whether each of 20 triplets lies on a semicircle.

Table 1: The Monte Carlo Simulation Techniques for Triplets of Random Numbers.

| No. | Triplet - 1 | Triplet - 2 | Triplet - 3 | Diff Max & Min | Diff New Max & Min | Triplet on Semi-Circle | Min Diff (x) |
|---|---|---|---|---|---|---|---|
| 1 | 0.21 | 0.11 | 0.71 | 0.60 | 0.90 | | 0.6 |
| 2 | 0.65 | 0.41 | 0.35 | 0.30 | | 0.3 | 0.3 |
| 3 | 0.17 | 0.91 | 0.07 | 0.84 | 0.90 | | 0.84 |
| 4 | 0.34 | 0.12 | 0.43 | 0.31 | | 0.31 | 0.31 |
| 5 | 0.38 | 0.49 | 0.13 | 0.36 | | 0.36 | 0.36 |
| 6 | 0.05 | 0.96 | 0.76 | 0.91 | 0.29 | 0.29 | 0.29 |
| 7 | 0.85 | 0.69 | 0.57 | 0.28 | | 0.28 | 0.28 |
| 8 | 0.63 | 0.41 | 0.03 | 0.60 | 0.62 | | 0.6 |
| 9 | 0.91 | 0.58 | 0.62 | 0.33 | | 0.33 | 0.33 |
| 10 | 0.75 | 0.89 | 0.23 | 0.66 | 0.48 | 0.48 | 0.48 |
| 11 | 0.21 | 0.36 | 0.59 | 0.38 | | 0.38 | 0.38 |
| 12 | 0.39 | 0.19 | 0.21 | 0.20 | | 0.2 | 0.2 |
| 13 | 0.74 | 0.86 | 0.90 | 0.16 | | 0.16 | 0.16 |
| 14 | 0.64 | 0.18 | 0.67 | 0.49 | | 0.49 | 0.49 |
| 15 | 0.20 | 0.72 | 0.34 | 0.52 | 0.86 | | 0.52 |
| 16 | 0.54 | 0.30 | 0.22 | 0.32 | | 0.32 | 0.32 |
| 17 | 0.48 | 0.74 | 0.76 | 0.28 | | 0.28 | 0.28 |
| 18 | 0.02 | 0.07 | 0.64 | 0.62 | 0.95 | | 0.62 |
| 19 | 0.95 | 0.23 | 0.91 | 0.72 | 0.32 | 0.32 | 0.32 |
| 20 | 0.48 | 0.55 | 0.91 | 0.43 | | 0.43 | 0.43 |
| **Total** | | | | | | **15** | **0.4** |

Out of 20 triplets, 15 were found to lie on a semicircle, yielding a calculated probability of $\frac{15}{20} = 0.75$. The experimentally determined value of $\pi$, where $N = 20$ and $n = 15$, was calculated as 3 using Equation 4:

$$\pi = \frac{4n}{N} \tag{4}$$

It was observed that increasing the sample size $N$ would bring the value of $\pi$ closer to its experimental value.

### 3.2 Friedman's Test Results

For the Friedman's test, the ranks of 20 randomly selected numbers were assigned row-wise for each Triplet – 1, Triplet – 2, and Triplet – 3, as illustrated in Table 2.

Table 2: Details of Ranks Assigned Row-wise for Each Triplet

| Sr. No | Triplet 1 | Triplet 2 | Triplet 3 | Rank of Triplet 1 | Rank of Triplet 2 | Rank of Triplet 3 |
|---|---|---|---|---|---|---|
| 1 | 0.21 | 0.11 | 0.71 | 2 | 1 | 3 |
| 2 | 0.65 | 0.41 | 0.35 | 3 | 2 | 1 |
| 3 | 0.17 | 0.91 | 0.07 | 2 | 3 | 1 |
| 4 | 0.34 | 0.12 | 0.43 | 2 | 1 | 3 |
| 5 | 0.38 | 0.49 | 0.13 | 2 | 3 | 1 |
| 6 | 0.05 | 0.96 | 0.76 | 1 | 3 | 2 |
| 7 | 0.85 | 0.69 | 0.57 | 3 | 2 | 1 |
| 8 | 0.63 | 0.41 | 0.03 | 3 | 2 | 1 |
| 9 | 0.91 | 0.58 | 0.62 | 3 | 1 | 2 |
| 10 | 0.75 | 0.89 | 0.23 | 2 | 3 | 1 |
| 11 | 0.21 | 0.36 | 0.59 | 1 | 2 | 3 |
| 12 | 0.39 | 0.19 | 0.21 | 3 | 1 | 2 |
| 13 | 0.74 | 0.86 | 0.90 | 1 | 2 | 3 |
| 14 | 0.64 | 0.18 | 0.67 | 2 | 1 | 3 |
| 15 | 0.20 | 0.72 | 0.34 | 1 | 3 | 2 |
| 16 | 0.54 | 0.30 | 0.22 | 3 | 2 | 1 |
| 17 | 0.48 | 0.74 | 0.76 | 1 | 2 | 3 |
| 18 | 0.02 | 0.07 | 0.64 | 1 | 2 | 3 |
| 19 | 0.95 | 0.23 | 0.91 | 3 | 1 | 2 |
| 20 | 0.48 | 0.55 | 0.91 | 1 | 2 | 3 |
| **Total of Ranks** | | | | **40** | **39** | **41** |

The null hypothesis assumes that all triplets exert identical effects, while the alternative hypothesis suggests that the effects vary among the triplets. Here, $N$ represents the total number of triplets (20), and $k$, the number of conditions, is 3. The total ranks for each column were 40, 39, and 41, respectively. The Friedman test statistic was calculated as 380.16 using Equation (5):

$$FM = \frac{12N}{k(k+1)} \left( \sum R^2 - \frac{k(k+1)^2}{4} \right) \tag{5}$$

With the significance level set at 5% and the degrees of freedom $df = k - 1 = 2$, the critical value from the Chi-Square table for 2 degrees of freedom at 5% significance is $FM_{\text{table}} = 5.99$. Given that the computed Friedman test statistic $FM_{\text{Calculated}} = 380.16$ significantly exceeds the critical value $FM_{\text{table}} = 5.99$, the null hypothesis is rejected. This result indicates significant differences in the effects of the triplets.

### 3.3 Chi-Square Goodness-of-Fit Test

The Chi-Square Goodness-of-Fit test was conducted to determine if the distribution of differences between maxima and minima across triplets aligns with a theoretical or expected distribution. The obtained results are shown in Table 3 The hypotheses were formulated as follows:

- Null Hypothesis ($H_0$): The observed distribution matches the expected distribution.
- Alternative Hypothesis ($H_1$): There is a significant difference between the observed and expected distributions.

The expected frequency ($E$) and the observed frequency ($O$) for each category were calculated, leading to the $\chi^2$ statistic using Equation (6).

$$\chi^2 = \sum \frac{(O - E)^2}{E} \tag{6}$$

With $N = 20$ triplets and the calculated $\chi^2$ value of 1.2977, we compare this to the critical value for 19 degrees of freedom at a 5% level of significance, 30.14. Since $1.2977 < 30.14$, we accept the null hypothesis, indicating no significant difference between the observed and expected distributions. This suggests that the triplets follow the expected goodness of fit, underscoring the importance of understanding both the statistical significance of test results and their practical implications in research contexts.

Table 3: Details of Observed and Expected Minimum Difference between Maxima and Minima

| Sr. No | Triplet - 1 | Triplet - 2 | Triplet - 3 | Difference between Maxima and Minima | Difference between New Maxima and New Minima | Minimum Difference between Maxima and Minima (O) | O-E | $(O-E)^2$ |
|---|---|---|---|---|---|---|---|---|
| 1 | 0.21 | 0.11 | 0.71 | 0.60 | 0.90 | 0.6 | 0.2 | 0.04 |
| 2 | 0.65 | 0.41 | 0.35 | 0.30 | | 0.3 | -0.1 | 0.01 |
| 3 | 0.17 | 0.91 | 0.07 | 0.84 | 0.90 | 0.84 | 0.44 | 0.194 |
| 4 | 0.34 | 0.12 | 0.43 | 0.31 | | 0.31 | -0.09 | 0.008 |
| 5 | 0.38 | 0.49 | 0.13 | 0.36 | | 0.36 | -0.04 | 0.002 |
| 6 | 0.05 | 0.96 | 0.76 | 0.91 | 0.29 | 0.29 | -0.11 | 0.0121 |
| 7 | 0.85 | 0.69 | 0.57 | 0.28 | | 0.28 | -0.12 | 0.014 |
| 8 | 0.63 | 0.41 | 0.03 | 0.60 | 0.62 | 0.6 | 0.2 | 0.04 |
| 9 | 0.91 | 0.58 | 0.62 | 0.33 | | 0.33 | -0.07 | 0.005 |
| 10 | 0.75 | 0.89 | 0.23 | 0.66 | 0.48 | 0.48 | 0.08 | 0.006 |
| 11 | 0.21 | 0.36 | 0.59 | 0.38 | | 0.38 | -0.02 | 0.0004 |
| 12 | 0.39 | 0.19 | 0.21 | 0.20 | | 0.2 | -0.2 | 0.04 |
| 13 | 0.74 | 0.86 | 0.9 | 0.16 | | 0.16 | -0.24 | 0.058 |
| 14 | 0.64 | 0.18 | 0.67 | 0.49 | | 0.49 | 0.09 | 0.008 |
| 15 | 0.2 | 0.72 | 0.34 | 0.52 | 0.86 | 0.52 | 0.12 | 0.014 |
| 16 | 0.54 | 0.3 | 0.22 | 0.32 | | 0.32 | -0.08 | 0.006 |
| 17 | 0.48 | 0.74 | 0.76 | 0.28 | | 0.28 | -0.12 | 0.014 |
| 18 | 0.02 | 0.07 | 0.64 | 0.62 | 0.95 | 0.62 | 0.22 | 0.048 |
| 19 | 0.95 | 0.23 | 0.91 | 0.72 | 0.32 | 0.32 | -0.08 | 0.006 |
| 20 | 0.48 | 0.55 | 0.91 | 0.43 | | 0.43 | 0.03 | 0.0001 |
| | | | | | | Total | 0.405 | 0.5256 |

# 4 Discussion

The Monte Carlo Simulation method was employed to estimate the value of $\pi$, utilizing random sampling within a geometric framework. The efficacy of this method is strongly influenced by the sample size $N$; an increase in $N$ leads to an estimated value of $\pi$ that converges more closely to its true value. This convergence is supported by the Law of Large Numbers, which asserts that the average of the results from a large number of trials will approximate the expected value. The Monte Carlo method involves generating pairs of random numbers and determining whether these points lie within a unit circle inscribed in a square. The ratio of points within the circle to the total number of points, multiplied by 4, yields an estimate of $\pi$. This approach is valued for its simplicity and computational efficiency, making it a popular choice for numerical integration and probabilistic simulations. To validate the distribution of the generated random numbers, non-parametric tests such as Friedman's Test and the Chi-Square Test were applied. Friedman's Test, which detects differences in treatments across multiple attempts, indicated that the triplets of random numbers have varying effects. This conclusion was derived by ranking the triplets and calculating the test statistic, which significantly exceeded the critical value at a 5% significance level, suggesting variability among the triplets and highlighting the stochastic nature of random sampling. The Chi-Square Test for goodness of fit assessed the alignment of the observed distribution of random triplets with the expected theoretical distribution. The calculated $\chi^2$ value was significantly lower than the critical value, leading to the acceptance of the null hypothesis. This indicates that the triplets of random numbers closely follow the expected distribution, affirming the reliability of the Monte Carlo Simulation method in generating random samples that conform to theoretical expectations. These findings underscore the importance of employing robust statistical methods to analyze and validate the results of simulations, confirming the effectiveness of the Monte Carlo method and the appropriateness of non-parametric tests in hypothesis testing for random samples.

# 5 Conclusions

This paper investigates the value of $\pi$ obtained through the Monte Carlo Simulation method and compares the results with the experimental value of $\pi$. It also tests the distribution of the Monte Carlo Simulation by applying non-parametric hypothesis testing methods, such as Friedman's Test and the Chi-Square Test. The detailed discussion and analysis provided offer significant insights into the application of these statistical techniques. Key findings include:

- **Accuracy of Monte Carlo Simulation:** The accuracy of the Monte Carlo Simulation improves with larger sample sizes $N$, underscoring the importance of scale in such simulations to achieve closer approximations of mathematical constants.
- **Effect of Random Triplets:** Friedman's Test reveals variability among triplets of random numbers, rejecting the null hypothesis that all triplets have identical effects. This finding is critical in considering the randomness and distribution of data points in simulations.

- **Goodness of Fit:** The Chi-Square Test confirms that the triplets of random numbers adhere well to the theoretical distribution, accepting the null hypothesis of goodness of fit and affirming the consistency of the Monte Carlo method with expected theoretical results.

These findings have broader implications for the fields of computational engineering and data science. By demonstrating the reliability and accuracy of Monte Carlo simulations in estimating $\pi$ and analyzing random distributions, this study provides a robust framework for students, researchers, and data analysts. The application of non-parametric tests like Friedman's Test and the Chi-Square Test provides powerful tools for hypothesis testing, enhancing informed decision-making based on empirical data. The methodologies and results discussed can serve as references for further research and applications in various domains where statistical analysis and simulations are pivotal. Understanding the behavior of random numbers and their distributions is crucial for optimizing algorithms, enhancing data analysis techniques, and improving the accuracy of computational models. In summary, this paper not only confirms the effectiveness of the Monte Carlo Simulation method in approximating $\pi$ but also highlights the importance of statistical hypothesis testing in validating simulation results. These contributions are expected to foster deeper insights and innovations in computational and statistical methods.

# 6 Acknowledgment

The authors are thankful to Management of Hope Foundation's Finolex Academy of Management and Technology, Ratnagiri, for providing excellent computational facilities. Authors also, thankful to unknown referees for their comment and suggestions to substantial improvement of quality of the paper.

# Declaration of Competing Interests

The authors declare that they have no known competing financial interests or personal relationships that could have appeared to influence the work reported in this paper.

# Funding Declaration

This research did not receive any grants from governmental, private, or nonprofit funding bodies.

# Author Contribution

**Sanjay Kulkarni**: Conceptualization, Methodology, Investigation, Visualization, Writing - original draft, review and editing. **Sandeep Kulkarni**: Investigation, Visualization, Resources.

# References

[1] Y. Dodge, *Statistical data analysis and inference*. Elsevier, 2014.

[2] C. Ismay and A. Y. Kim, *Statistical Inference via Data Science*. 2019.

[3] J. S. Milton and J. C. Arnold, *Introduction to Probability and Statistics*. 2007.

[4] R. A. Johnson and C. B. Gupta, *Probability and Statistics for Engineers*. 2007.

[5] A. Chandrasekaran and G. Kavitha, *Probability Statistics Random Processes and Queuing Theory*. 2014.

[6] P. Bruce and A. Bruce, *Practical Statistics for Data Scientists*. 2017.

[7] J. A. Rice, *Mathematical Statistics and Data Analysis*. Thomson Higher Education, 2013.

[8] Z. Liu, F. Blasch, and V. Jhon, "Statistical comparison of image fusion algorithms recommendations," *Inf. Fusion*, 2017.

[9] S. Couch, Z. Kazan, K. Shi, A. Bray, and A. Groce, "Differentially private nonparametric hypothesis testing," in *Proc. Of the ACM Conf. Comput. Commun. Secur.*, 2019.

[10] S. García, A. Fernández, J. Luengo, and F. Herrera, "Advanced non-parametric tests for multiple comparisons in the design of experiments in computational intelligence and data mining: experimental analysis of power," *Inf. Sci.*, 2010.

[11] S. D. Pawar and D. T. Shirke, "Nonparametric tests for multivariate multi-sample locations based on data depth," *J. Stat. Comput. Simul.*, 2019.

[12] J. Derrac, S. García, S. Hui, P. N. Suganthan, and F. Herrera, "Analyzing convergence performance of evolutionary algorithms: a statistical approach," *Inf. Sci.*, 2014.

[13] J. Demšar, "Statistical comparisons of classifiers over multiple data sets," *J Mach Learn Res.*, vol. 7, no. 1, 2006.

[14] R. G. D. Steel, "A multiple comparison sign test: treatments versus control," *J. Am. Stat. Assoc.*, 1959.

[15] K. Doksum, "Robust procedures for some linear models with one observation per cell," *Ann. Math. Stat.*, 1967.

[16] T. B. Chandra, K. Verma, B. K. Singh, D. Jain, and S. S. Netam, "Coronavirus disease (covid-19) detection in chest x-ray images using majority voting-based classifier ensemble," *Expert Syst. Appl.*, 2021.

[17] M. De Gregorio and M. Giordano, "An experimental evaluation of weightless neural networks for multi-class classification," *Appl. Soft Comput. J.*, 2018.

[18] F. J. Pulgar, F. Charte, A. J. Rivera, and M. J. Del Jesus, "Choosing the proper autoencoder for feature fusion based on data complexity and classifiers: analysis, tips and guidelines," *Inf. Fusion*, 2020.

[19] S. Shi, S. Ding, Z. Zhang, and W. Jia, "Energy-based structural least squares mbsvm for classification," *Appl. Intell.*, 2020.

[20] J. Liu, "Fuzzy support vector machine for imbalanced data with borderline noise," *Fuzzy Sets Syst.*, 2020.

[21] M. Petrović, Z. Miljković, and A. Jokić, "A novel methodology for optimal single mobile robot scheduling using whale optimization algorithm," *Appl. Soft Comput. J.*, 2019.

[22] T. W. O'Gorman, "A comparison of the f-test, friedman's test, and several aligned rank tests for the analysis of randomized complete blocks," *J. Agric. Biol. Environ. Stat.*, 2001.

Journal of Computers, Mechanical and Management
Journal homepage: www.jcmm.co.in
e-ISSN: 3009-075X
AN PUBLISHING

Volume 3 Issue 1

**Article Number:** 240117

# A Review of Nondestructive Testing Methods for Aerospace Composite Materials

Md. Shaishab Ahmed Shetu*

Department of Aeronautical and Aviation Science and Engineering, College of Aviation Technology, National University of Bangladesh, Gazipur, Dhaka, Bangladesh 1230

**Abstract**

Composite structures and materials have seen significant advancements in cost-effectiveness, product efficiency, and specific properties, leading to their extensive use in the aerospace industry. Reliable nondestructive testing (NDT) of composites is crucial for reducing maintenance costs and addressing safety concerns. This review provides a comprehensive analysis of various NDT methods, including Ultrasonic Testing, Acoustic Emission, Eddy Current Testing, Shearographic Testing, Infra-Red Thermography, and X-Ray Radiography. Each method's principles, instruments, and applications for defect detection and damage evaluation in composite materials are thoroughly examined. The paper highlights the strengths and limitations of these NDT techniques, emphasizing their roles in ensuring the structural integrity of aerospace composites. Ultrasonic Testing and Infra-Red Thermography are identified as flexible and cost-effective solutions, widely applied in both academic research and industrial sectors. Despite the challenges in providing a complete diagnostic of structural integrity, each NDT method offers unique advantages. Future research in NDT for composites will focus on integrating advanced data processing techniques, such as machine learning and deep learning, and developing smart inspection systems with high precision and rapid data processing capabilities.

**Keywords:** Non-Destructive Testing; Composite Material; Ultrasound; Shearography; Inspection

## 1 Introduction

The first aircraft developed by the Wright Brothers was constructed using natural composites such as wood. However, it was not until the invention of carbon fiber in 1964 that composites began to be extensively adopted as primary and secondary structural materials in aircraft [1]. The objective was to develop innovative, lightweight, stiff, and robust materials suitable for aircraft structures. Carbon Fiber Reinforced Polymers (CFRP), which consist of carbon fibers embedded within a polymer matrix, have become increasingly popular due to their exceptional strength-to-weight ratio, corrosion resistance, and the capability to fabricate components with complex geometries. These attributes have led to their widespread use, particularly in the aerospace industry [2]. Nevertheless, periodic testing is essential throughout the operational life of an aircraft to ensure the structural integrity and safety of its composite components. The proliferation of composite materials in aircraft parts such as wing skins, engine covers, and fuselages has introduced unforeseen challenges. For example, T-shaped stringer elements are utilized to reinforce the CFRP shells of aircraft [3]. These stringers require a secondary polymerization process, as they are partially embedded within the aircraft's CFRP shell [4]. Improper polymerization conditions can lead to crack initiation in these stringers. Another significant challenge is the automated fiber placement technique, which involves the robotic layering of pre-impregnated fibers on a composite panel. This method can introduce defects such as gaps, laps, and twists [5].

*Corresponding author: shaishab.ahmed185365@gmail.com
**Received:** 10 February 2024; **Revised:** 15 February 2024; **Accepted**: 21 February 2024; **Published:** 29 February 2023

**DOI:** 10.57159/gadl.jcmm.3.1.240117.

Furthermore, hybrid materials combining aluminum alloys and CFRP are now employed in aircraft components like nacelles, wing boxes, and fuselages due to their superior fatigue life, impact resistance, and residual strength properties [6]. The complexity of these components, due to their numerous interfaces, complicated geometries, and diverse elastic properties, makes them difficult to inspect. Additionally, components are often replaced or repaired to extend the lifespan of aging aircraft when damage is minor. A method involving the application of composite patches has been shown to reduce operating costs. Moreover, composites can develop internal defects during manufacturing and throughout their service life. Impacts are a common cause of in-service defects [7, 8]. Even low-energy impacts can result in Barely Visible Impact Damage (BVID), which often leads to a complex network of matrix cracking and delamination internally or on the reverse side without altering the structure's exterior surface [9–11, 6]. Such damage poses a significant risk as it is not visually detectable and can be challenging to identify during routine inspections [12].Other internal defect mechanisms, such as porosity, matrix cracking, delaminations, and inclusions, may also contribute to the failure of composite structures in addition to impact-induced damages [13, 8]. Numerous Non-Destructive Testing (NDT) methods have been developed for diagnostic applications in aerospace composites. This paper reviews advancements in the field, critically evaluating the advantages and disadvantages of each method. In particular, it addresses innovative NDT systems that hold promise for overcoming the challenges associated with damage characterization and detection in composite laminates. These challenges include high aspect ratios, complex geometry, and limited access due to varying elastic properties. The application of smart inspection techniques is proposed to mitigate these difficulties. As outlined in Table 1, various Non-Destructive Testing (NDT) techniques offer specific capabilities and face particular limitations that are critical in their application to aerospace composites.

Table 1: Comparison of Non-Destructive Testing (NDT) Techniques Highlighting Their Capabilities and Limitations in Aerospace Applications

| **NDT Techniques** | **Capabilities** | **Limitations** |
|---|---|---|
| **UT (Ultrasonic Testing)** | Capable of identifying surface and subsurface anomalies. | Small anomalies smaller than the grain size may go unnoticed. Largely manual, heavily reliant on the expertise and experience of the operator. Signal misinterpretations can occur. |
| **AE (Acoustic Emission)** | Able to detect surface and subsurface flaws and provide details on the progression of the anomaly. | Extrinsic noises can lead to misinterpretations. Stress vibrations may be attenuated by the structure being tested. |
| **ECT (Eddy Current Testing)** | Effective in detecting defects in electrically conductive materials, including those that are coated, primarily on or near the surface. | Limited in assessing subsurface abnormalities in ferromagnetic materials. Restricted to the evaluation of elements with electrical conductivity. |
| **ST (Shearography)** | Efficient in examining disbands and Barely Visible Impact Damages (BVIS). | The material must be subjected to external stressors such as vacuum, pressure, vibration, or heat. |
| **IRT (Infrared Thermography)** | Capable of identifying impact-induced defects such as matrix microcracks, fiber breakage, and delamination. | Limited to near-surface defect imaging; effectiveness depends highly on defect depth and size. |
| **X-Ray** | Primarily used to identify cracks developing in a plane perpendicular to the beam direction and to detect mesoscale and macroscale damage in composite laminates. | Conventional X-rays have limited contrast for common radiographic defects in aerospace composites, restricting their effectiveness. |

## 2 Ultrasonic Testing

As shown in Figure 1, ultrasonic testing (UT) is an acoustic inspection technique that utilizes the reflection and transmission of elastic waves within composite materials to identify defects. This method spans a broad frequency range from 20 kHz to 1 GHz, tailored to specific applications. The frequency range most commonly employed in industry for Non-Destructive Testing (NDT) varies between 0.5 and 10 MHz, although frequencies up to 100 MHz are utilized specifically for detecting matrix cracks [14]. UT employs several representation methods, namely A-scan, B-scan, C-scan, and D-scan [14]. The C-scan method is particularly effective for monitoring transmission losses caused by disbands and delaminations under both low-energy and high-energy impacts [15–17]. During ultrasonic inspections, the sound beam aligns with the axis of the reinforcement fibers, efficiently characterizing misalignments. Delaminations and debonding result in discrete reflections and transmission losses from specific material depths.

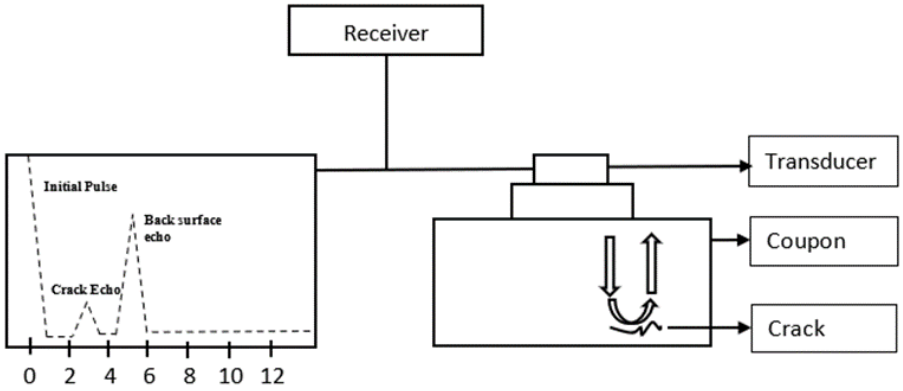


Figure 1: Schematic representation of Ultrasonic Testing [18]

Conversely, porosity leads to the scattering of ultrasonic waves rather than discrete reflections, thus causing transmission losses [8]. Studies have demonstrated that the attenuation of waves propagating perpendicular to CFRP plies can yield crucial information for assessing and interpreting interlaminar quality. Both time domain and frequency domain signal processing techniques are employed to distinguish defect echoes from the multiple reflections occurring within the composite. This aids in localizing defects and enhances the probability of detecting them [18–21]. To address the challenges associated with rough surfaces and non-parallel layers in multi-material joints, a novel signal post-processing method has been developed [22]. A common technique employed in such scenarios is ultrasonic immersion testing, which involves coupling sound waves through a liquid medium to inspect the material. This method is particularly effective where there is a significant mismatch between air and solid materials [23, 24]. Typical frequencies used depend on the composite layer being inspected. Frequencies as low as 0.5 MHz are used for inspecting composites up to 50 mm thick, such as glass/epoxy materials. Swept frequencies ranging from 0.4 to 1.0 MHz have been employed to inspect 25.4 mm thick Glass Fiber Reinforced Polymer (GFRP) composites. Additionally, frequencies between 100 kHz and 400 kHz using air-coupled ultrasound have proven effective for inspecting 48 mm thick glass fiber/polyester resin composites [25]. Despite its extensive applications, ultrasonic testing encounters several limitations. For instance, a shadow effect can obscure larger delaminations near the surface, as these large discontinuities reflect sound and reduce visibility below the delamination [15]. Furthermore, UT faces significant challenges in detecting discontinuities within non-homogeneous materials, such as popular honeycomb composites, due to the mismatch between air and solid materials [15].

## 3 Acoustic Emission

Acoustic Emission (AE) is an inspection method that utilizes the sound waves generated by a material under stress to detect flaws. These sound waves, known as stress waves, interact with any discontinuities within the material, altering their amplitude and speed. Inspectors detect these changes to locate flaws. The working principle of AE is illustrated in Figure 2 [26]. Figure 2 depicts pictographically the principle of AE. In composite materials, events such as fiber breakage, matrix cracking, and fiber misalignment lead to the sudden release of stress waves [27–29]. AE techniques utilize a series of piezoelectric interdigital transducers or sensors to capture these stress waves. These sensors convert the stress waves into electrical signals, which can then be analyzed by inspectors. AE is distinct because the stress waves are emitted by the material itself, not from an external source. This technique not only records displacement data but also monitors the dynamic processes within a composite material, tracking the evolution of specific defects and providing valuable information during fatigue testing [30].

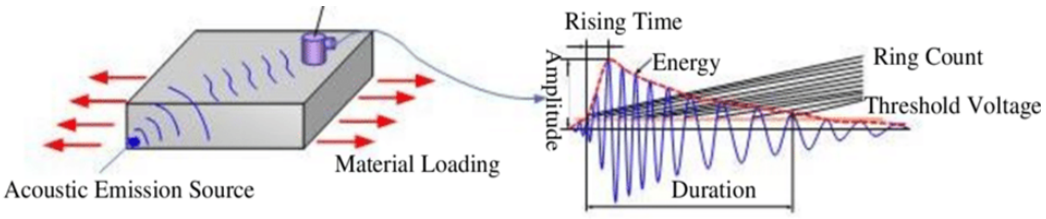


Figure 2: Principle of Acoustic Emission Testing [31]

Features extracted from the AE waveform, typically in the time range specified in studies [27, 31, 32], along with AE spectra [33], are crucial for Non-Destructive Testing of composite structures. These features can facilitate a classification system that assesses the current condition of the component. However, AE testing presents several challenges. Each AE event produces a unique stress wave that cannot be halted or replicated. For example, the slow growth of a crack might generate a weak signal, whereas a rapid expansion of a similar crack could produce a more pronounced, albeit temporary, signal [34]. The data collected during AE testing can vary, with amplitude signals being the most common.

The range of ultrasound frequencies used in AE spans from 20 kHz to 1 MHz. Processing and analyzing this data requires specific expertise and is time-consuming. Overlaps in the amplitude distributions can also complicate the correlation with specific damage mechanisms. To address these challenges, researchers have explored multiple parameters to enhance damage analysis, such as the duration or frequency of amplitude signals [35, 36], cumulated event count [37, 38], and energy [39]. Additionally, microscopy is often used to confirm damage modes and ensure accurate analysis. Several ASTM standards govern the use of AE in testing composite materials: ASTM E1067 for examining glass fiber-reinforced plastic tanks/vessels under a maximum internal pressure of 1.73 MPa; ASTM E1118 for composite pipes under pressures up to 35 MPa; ASTM E2191 for filament wound composite pressure vessels tested up to 68.9 MPa; ASTM E2076 for composite fan blades; and ASTM E2661 for materials containing continuous high modulus fibers greater than 20 MPa, such as plate-like and flat composite structures in aerospace applications [40].

# 4 Eddy Current Testing (ECT)

Eddy current testing (ECT) is an electromagnetic testing method that utilizes electromagnetic induction to inspect surface and sub-surface flaws in composite materials. Recent studies have demonstrated that eddy currents can be employed to review conductive composite materials such as Carbon Fiber Reinforced Plastics (CFRP) and metal matrix composites. ECT is classified into two types: pulsed ECT and remote ECT. Pulsed ECT is utilized to detect flaws in conductive materials. It has been shown to be effective for inspecting conductive composite materials like metal-matrix composites and CFRP [6]. Eddy currents are particularly well-suited for detecting low-energy impact damage, thermal damage, fiber damage with or without matrix cracking, and other types of damage affecting the fibers in the sample material. In CFRPs, ECT measurements specifically respond to carbon fibers [41–43]. The principle of ECT is based on the fluctuation of the magnetic field caused by eddy currents. Figure 3 [44] illustrates a typical ECT set-up, which consists of two circuits: a primary and a secondary circuit. In this set-up, the primary circuit is connected to an AC supply, establishing a primary fluctuating magnetic field that induces eddy currents in the experimental object. These eddy currents generate a secondary magnetic field that interferes with the primary magnetic field, thereby impacting the current flowing through the coil. Changes in the eddy currents alter the current configuration caused by the secondary magnetic field, consequently modifying the primary current. This variation results in a change in the impedance reading, indicating a discontinuity.

ECT employs both high and low frequencies, each generating different fields. The High-Frequency Eddy Current Technique (HFECT) was developed to visualize fiber orientation, fiber fraction changes, resin-rich regions, delamination, and impact damage in CFRP composites [45]. HFECT is better suited for less conductive materials. When high frequencies, such as 50 MHz or above, are used, only near-surface defects can be described due to limited penetration depth to the top few plies below the sample surface [41]. Conversely, low-frequency ECT is more commonly used for sandwich structures, allowing for a higher evaluation of the sample material's integrity at lower frequencies. The development of a high-precision low-frequency ECT up to 250 kHz enabled the identification and visualization of several defects, including fiber orientation, misaligned fiber bundles, cracks, delamination, and impact damage in scanned images [46].

Despite its capabilities, ECT has limitations in non-destructive testing for detecting surface and sub-surface defects in CFRPs due to its limited penetration depth. Interpreting measured signals can be challenging, as distinguishing interlaminar fractures from delamination can be difficult. This method is applicable only to composites made of conductive fibers, such as carbon fiber, and is often modified to work with less conductive structures [15]. The lift-off effect, caused by variations in the distance between the probe and the test sample, as well as the need to consider the surface status, refers to changes in the mutual inductance between the excitation coil and the test sample [47].

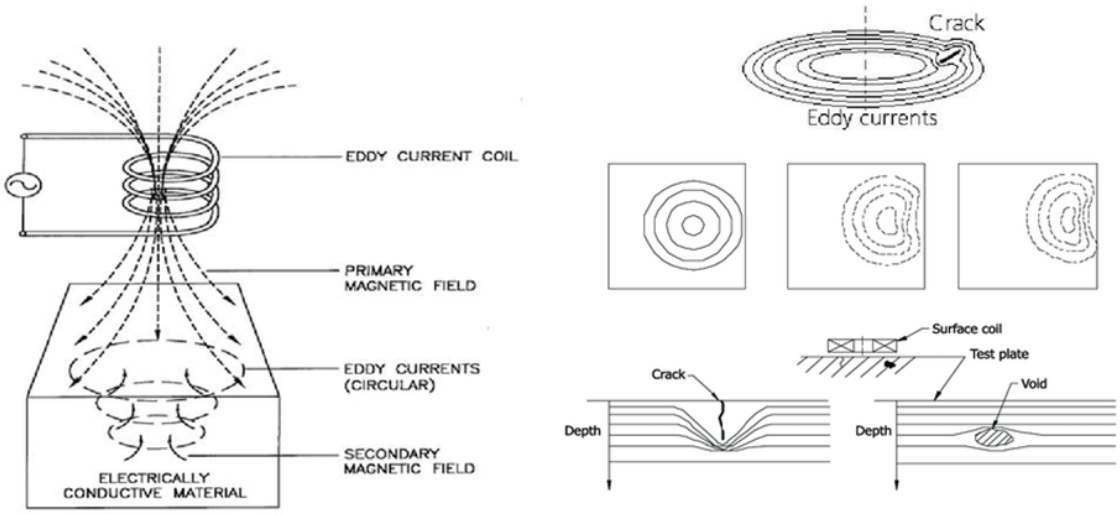


Figure 3: Schematic diagrams of Eddy Current Testing (ECT) set-ups showing primary and secondary magnetic fields, eddy currents, and typical crack detection scenarios [44].

# 5 Shearographic Testing (ST)

Shearography is a laser-based optical technique [48]. To introduce image shearing in digital shearography, a shearing device must be placed in front of the camera. This setup allows light reflected from two distinct object points to interfere at a single point in the image plane [49]. Various shearing instruments, including an optical wedge or biprism, a Mach-Zehnder interferometer [50], and an updated Michelson interferometer, have been used in digital shearography evaluations. The modified Michelson interferometer is the most popular shearing device due to its simple structure and ease of adjusting the shearing amount and orientation.

The conventional shearographic configuration in Figure 4 [49] produces interference at point P and determines the shearing amount using a modified Michelson interferometer. By slightly moving mirror 1, the shearing effect can be achieved. Point P on the sensor plane can then receive light waves from locations P1 and P2 on the object's surface. A speckle pattern, also known as a speckle interferogram, is produced when these light pulses collide, and the resulting pattern is recorded by a CCD camera and stored in the computer. Further improvements can be achieved using a loading system and quantitative evaluation methods.

There are four shearographic methods that utilize a loading system to inspect composite materials: Pressure Shearography, Heat Pulse Shearography, Vibration (Acoustic) Shearography, and Vacuum Shearography. Shearography is widely adopted in aeronautics for evaluating composite parts. When used in the aerospace sector, Shearography offers several advantages, such as high speed and real-time monitoring of large composite panels [51, 52]. Due to these benefits, Shearography is currently used for Non-Destructive Testing (NDT) on various aircraft, including the NASA space shuttle, the F-22, the F-35 JSF, the Airbus, the Cessna Citation X, and the Airbus [53].

Shearography is primarily employed to detect debonding or the initiation of delamination, as stress concentrations around a particular defect intensify the failure risk of composites [54–59]. However, Shearography has significant disadvantages, such as the difficulty in characterizing fiber breakage, matrix cracking, or matrix/fiber debonding (i.e., microscopic to mesoscopic damage mechanisms). Additionally, its sensitivity to environmental disturbances makes it challenging to apply in industrial operations [60].

To help identify specific defects, Shearography is sometimes combined with other non-destructive evaluation methods [61]. Utilizing double pulse laser illumination (spatial stage modulation) and stroboscopic laser (temporal stage modulation) can also enhance damage localization in Shearography [62]. Both excitation techniques are employed to detect delaminations; however, the latter method yields better results due to noise reduction in the maps of the temporal phase modulation. Research indicates that fuzzy neural analysis can significantly improve the ability to identify delamination in composite materials [63].

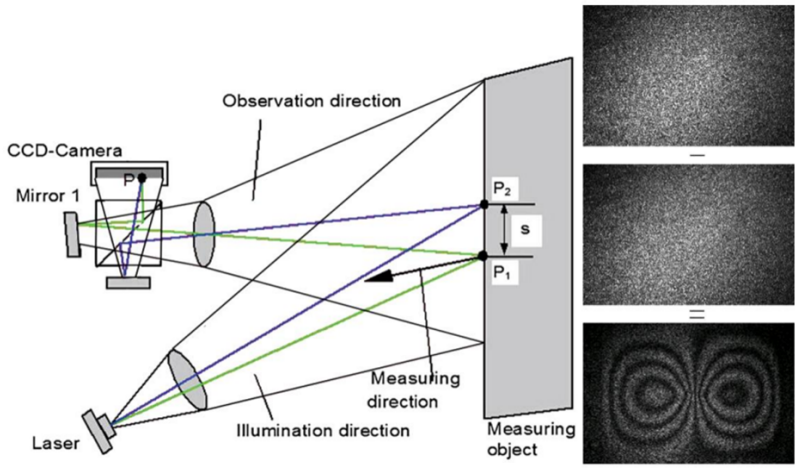


Figure 4: Schematic diagrams of Shearographic Testing (ST) set-ups showing image shearing using a modified Michelson interferometer [49].

# 6 Infra-Red Thermography (IRT)

Infra-Red Thermography (IRT) is a technique that uses thermal distributions to map and measure infrared energy emissions from an object. Infrared energy, which is electromagnetic radiation with longer wavelengths than visible light, is emitted by every object with a temperature above absolute zero [64]. Over the past few decades, IRT has rapidly advanced with improvements in infrared cameras, data acquisition, and processing methodologies. It offers capabilities such as non-contact, non-invasive, real-time measurement, high resolution, and the ability to cover large areas [65].

In IRT testing, a thermal gradient is produced due to varying emissivity coefficients when thermal energy diffuses through an object and encounters material defects such as porosity, matrix cracking, delaminations, and inclusions. This thermal gradient can be used to assess the damage [66]. A surface temperature map of the structure under examination is obtained by analyzing the thermal output of the material in the infrared electromagnetic band of the employed detector

(infrared camera), as shown in Figure 5 [67]. Consequently, it is feasible to identify flaws in composites, especially if their thermal properties differ significantly from those of the base material.

IRT-based Non-Destructive Testing (NDT) has been widely used in both Boeing and Airbus for structural health monitoring to ensure the functionality of their composite products. NASA has utilized IRT for many years to examine manned flight vehicles during orbit inspection [68]. Numerous researchers have also explored the use of IRT to quickly examine large aerospace components, including jet engines, spacecraft parts and their subsystems, and aircraft primary and secondary structures [69–72]. Current field research is investigating the development of robotized line scan thermography methods to inspect large composite structures [71, 73].

IRT is typically classified into two types: "passive" and "active" thermography [74]. In passive thermography (PT), thermal radiation is directly emitted from the test body's surfaces under ambient conditions and then observed. In active thermography (AT), a heating or cooling flow is generated and propagated into the test object to reveal internal structures. Thermal responses in accordance with the Stefan-Boltzmann law are then detected and documented. Recent advancements in signal processing techniques and equipment have made the AT method more practical and efficient than the traditional PT strategy [75, 76].

Active IRT is generally divided into optically stimulated thermography [77], ultrasonic stimulated thermography [77–79], eddy current stimulated thermography [80], and metal-based thermography, depending on the external heat source used [81]. The most frequently used setup in the IRT of aerospace structures is optically stimulated thermography. Pulsed or transient thermography is a popular optical technique for aerospace applications. Research has shown that local material non-uniformities, which cause small variations in thermal energy, can prevent thermography from accurately measuring the entire extent of the delaminated zone [82]. Additionally, it has been documented that the temperature contrast on composite laminates diminishes as the orientation angles between adjacent layers become more varied [83]. As a result, cross-ply or multi-angle ply laminates are more challenging to examine for flaws than unidirectional laminates, particularly when thick laminates made from CFRP are reinforced with high thermal conductivity fibers [84].

While higher aspect ratios are anticipated in aerospace applications, the aspect ratio of the defects at the detection limit is between two and three [85]. Therefore, IRT is restricted to near-surface damage identification with low aspect ratios in both impact-induced and machining-induced defects. The technique is not particularly sensitive to in-depth damage and microcracks with sizes varying from ten microns to a few millimeters [70, 86].

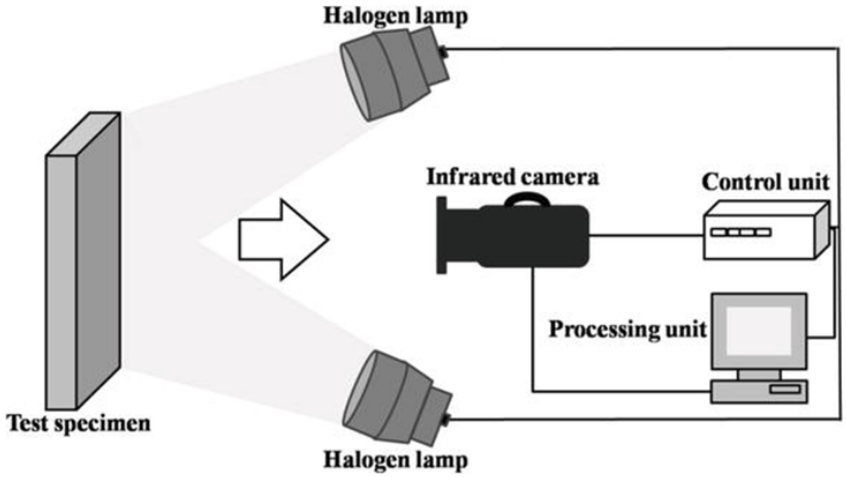


Figure 5: Schematic diagrams of Infra-Red Thermography (IRT) showing thermal distributions and defect detection [67].

# 7 X-Ray Radiography

X-ray radiography is based on the characteristics of radiation, which are waves or electrons emitted from a source that travel through a medium. The Beer-Lambert rule explains how X-rays of a particular energy interact with matter. In X-ray radiography, short wavelength electromagnetic radiations (high-energy X-ray photons) penetrate different materials to produce a shadowgraph image of the test object. The attenuation of X-ray radiation as it travels through the object toward an X-ray detector is affected by the test object's density, path length, and level of X-ray absorption. Conventional radiography is widely used to identify non-planar defects in aerospace composites, such as solid inclusions, fiber misalignment, and matrix cracking, provided the orientation of these defects is not perpendicular to the X-ray beam [61, 87].

Conventional radiography uses penetrating X-rays to examine the internal structure of composite materials. A 2D image, known as an X-radiograph, is created by projecting the attenuated beam onto an X-ray-sensitive film or a digital scanner. The X-radiograph displays the attenuation of X-rays due to variations in electron density along the beam path. Radiography can detect translaminar cracks and delamination, as well as meso- and macroscale damage to composite laminates [88]. However, it primarily enables the detection of cracks developing in a plane perpendicular to the path of the beam [89]. Figure 6 illustrates the principles of gamma radiography [90].

For thin components (less than 5 mm in thickness), low-voltage radiography is used, while thicker parts are better

suited for gamma-ray radiography. When defects overlap and are superimposed onto a planar surface, they cannot be separated, and depth quantification is not feasible without multiple radiographs. Applying a dye penetrant before inspection can enhance the ability to identify microscale damage mechanisms, such as matrix cracking, if the cracks are linked to the material's surface. Guild et al. [91] used penetrant-enhanced radiography to track the initiation and propagation of matrix cracking in pre-notched carbon/epoxy laminates subjected to tensile fatigue loading. Additionally, Atas et al. [92] identified and monitored the development of subcritical damage processes in CFRP joints.

More sophisticated methods, such as X-ray Computed Tomography (XCT or CT) and X-ray Computed Laminography (XCL or CL), have been developed from traditional X-radiography to visualize interior features within components and obtain digital data on their three-dimensional geometries. These techniques shift the scale of Non-Destructive Testing (NDT) from macroscopic to microscopic, showing promise for resolving the current challenges in monitoring highly sensitive aerospace materials.

X-ray tomography (µCT) differs from traditional radiography methods in that it relies on the computerized reconstruction of a series of radiographs taken by rotating the sample at controlled angular steps. The resulting data is coded in greyscale and corresponds to 3D maps of elementary basic elements (referred to as voxels). The differences in the linear attenuation coefficients of the material's constituents (such as matrix, fiber, and porosity), where elements with high atomic numbers are the most absorbent and elements with low atomic numbers or low density, such as air cavities, are the least absorbent, are reflected in the grey level contrasts within the 3D images produced by standard laboratory µCT equipment. Consequently, if the difference between the linear absorption coefficients is large enough, it is possible to distinguish between the various components of the composite and locate the damage.

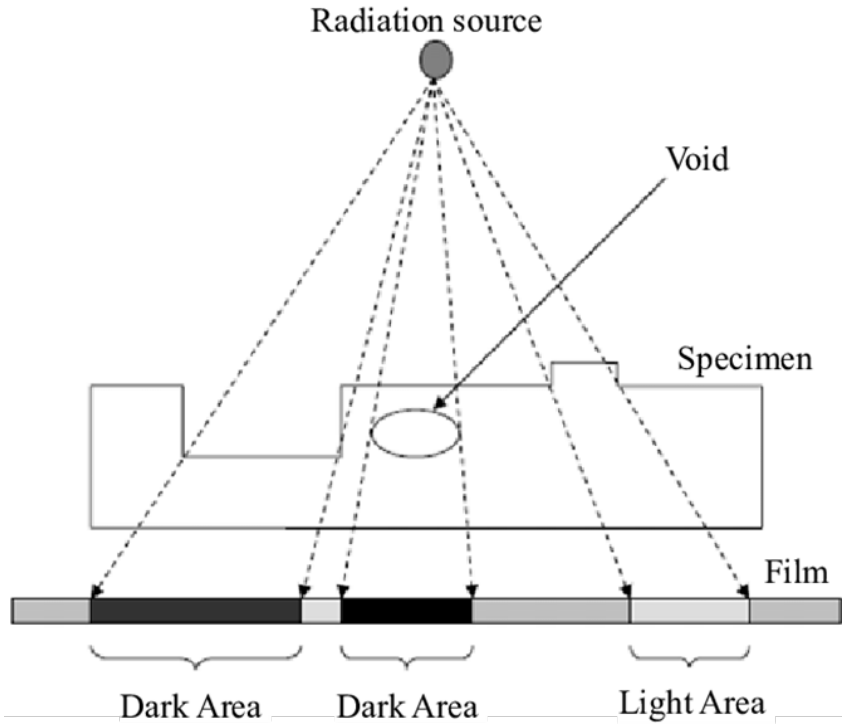


Figure 6: Schematic diagrams illustrating the principles of gamma radiography [90].

# 8 Discussion

The advancements in nondestructive testing (NDT) techniques have significantly enhanced the ability to monitor and evaluate composite materials. This review provides a comprehensive analysis of various NDT methods, highlighting their unique strengths, limitations, and applications. The novelty of this review lies in the comparative analysis and integration of advanced data processing techniques, such as machine learning and deep learning, with traditional NDT methods. One of the most significant advancements in NDT is the incorporation of machine learning (ML) and deep learning (DL) algorithms. These technologies can process large datasets, identify patterns, and predict outcomes with high accuracy. Integrating ML and DL with NDT methods enhances defect detection, characterization, and evaluation. For instance, algorithms can be trained to recognize specific defect signatures in ultrasonic testing (UT) or interpret complex thermal patterns in infrared thermography (IRT). This capability reduces human error and increases the reliability of NDT evaluations. The integration of multiple NDT techniques addresses the limitations of individual methods, providing a more comprehensive assessment of composite materials. For example, combining X-ray radiography with ultrasonic testing allows for detailed internal and surface defect analysis. The synergy of different NDT techniques enables the detection of a broader range of defects, from surface cracks to deep-seated flaws, thus ensuring more robust structural health monitoring. The development of smart materials with embedded sensors is another novel aspect discussed in this review. These materials can continuously monitor their own condition and provide real-time data on stress, strain, and

other critical parameters. Embedded sensors enhance the capabilities of traditional NDT methods by offering continuous and in-situ monitoring, leading to more accurate and timely assessments of material health. Technological advancements have also led to the creation of portable and handheld NDT devices. These innovations allow for in-field inspections, providing real-time data that can be crucial for immediate decision-making. Portable devices, coupled with advanced data processing techniques, can perform complex analyses on-site, reducing the need for laboratory-based testing and speeding up the inspection process. Despite these advancements, several challenges remain. The complexity of interpreting data from integrated NDT techniques, the need for high-resolution imaging, and the development of cost-effective solutions are ongoing research areas. Future directions include the further integration of AI and machine learning, the development of more sophisticated sensors, and the creation of standardized protocols for multi-NDT applications. These advancements will enhance the accuracy, efficiency, and applicability of NDT methods in various industries.

# 9 Conclusion

Nondestructive testing (NDT) techniques are essential resources for testing and assessment at various points in a composite product's lifecycle. While every technique has potential, only a few can fully diagnose potential flaws and the evolution of damage in a composite system. The strengths and weaknesses of the reviewed NDT methods are shown in Table 1. Selecting the appropriate NDT method can be challenging, yet it is crucial for preserving the structural integrity of composite materials and structures. The applications and capabilities of each reviewed NDT technique for identifying and evaluating defects and damage evolution in composite materials/structures are summarized.

As the volume and structural complexity of composite parts increase, the use of multi-NDT techniques is becoming more common for maintaining structural integrity, and research in this area is expanding significantly. The initial development and application of various NDT techniques were driven by demands in the aerospace industries, which have rapidly expanded to other fields. The main techniques used in the composite industries are X-ray radiography, acoustic emission, ultrasonic testing, infrared thermography, shearography, eddy current testing, and thermography. NDT techniques based on ultrasound, IRT, and AE are adaptable and cost-effective solutions that have been used extensively in many industrial fields and academic research.

GHz waves can penetrate opaque materials and detect internal defects and damage. Innovation and technological advances in small and portable NDT devices will continue to play a significant role in future NDT equipment, offering in-service inspections to aid the decision-making process. Although X-rays are highly effective NDT instruments with high resolution, the method is more expensive than other non-destructive testing approaches due to its reliance on ionizing radiation. The accessibility and cost of radiation facilities are further hampered by their limited locations and availability.

When used in non-destructive testing for identifying surface and subsurface defects in CFRPs, ECT has several drawbacks. For instance, it can be challenging to differentiate between interlaminar fractures and delamination from measured signals. This technique is limited to composite materials composed of conductive fibers. Considering the complex nature of flaws and damage identification in composites, the future development of NDT techniques will increasingly depend on smart inspection systems with high precision and effectiveness in data processing. Machine learning and deep learning show tremendous potential for the NDT evaluation of composite materials. Artificial intelligence–based systems allow quick decision-making without human interference. Numerous automated diagnostics for various NDT techniques have been developed, using algorithms for the automatic identification and recognition of flaws or damage, or by coding artificial neural networks.

NDT techniques have made significant progress, but much more work is required to provide quick and inexpensive systems for both data processing and equipment to support their practical application in industry.

# Declaration of Competing Interests

The author declares that he has no known competing financial interests or personal relationships that could have appeared to influence the work reported in this paper.

# Funding Declaration

This research did not receive any grants from governmental, private, or nonprofit funding bodies.

# Author Contribution

**Md. Shaishab Ahmed Shetu**: Conceptualization, Investigation, Data curation, Writing - original draft, review and editing.

# References


[1] C. Soutis, "Fibre reinforced composites in aircraft construction," *Progress in Aerospace Sciences*, vol. 41, no. 2, pp. 143–151, 2005.

[2] A. Katunin, K. Dragan, and M. Dziendzikowski, "Damage identification in aircraft composite structures: A case study using various non-destructive testing techniques," *Composite Structures*, vol. 127, pp. 1–9, 2015.

[3] H. Towsyfyan, A. Biguri, R. Boardman, and T. Blumensath, "Successes and challenges in non-destructive testing of aircraft composite structures," *Chinese Journal of Aeronautics*, vol. 33, no. 3, pp. 771–791, 2020.

[4] U. Ewert *et al.*, "Mobile computed tomography for inspection of large stationary components in nuclear and aerospace industries," *Materials Transactions*, vol. 53, no. 2, pp. 308–310, 2012.

[5] K. E. Cramer, "Current and future needs and research for composite materials nde," vol. 1059603, p. 500, 2018.

[6] X. Li, "Eddy current techniques for non-destructive testing of carbon fibre reinforced plastic (cfrp)," pp. 725–728, 2013.

[7] H. Kim, "Impact damage formation on composite aircraft structures," in *Federal Aviation Administration JAMS 2012 Technical Review Meeting*, pp. 1–58, 2012.

[8] R. A. Smith, "Composite defects and their detection," vol. III.

[9] X. E. Gros, "An eddy current approach to the detection of damage caused by low-energy impacts on carbon fibre reinforced materials," *Materials & Design*, vol. 16, no. 3, pp. 167–173, 1995.

[10] C. Soutis, "Carbon fiber reinforced plastics in aircraft construction," *Materials Science and Engineering: A*, vol. 412, no. 1–2, pp. 171–176, 2005.

[11] A. Katunin, K. Dragan, and M. Dziendzikowski, "Damage identification in aircraft composite structures: A case study using various non-destructive testing techniques," *Composite Structures*, vol. 127, pp. 1–9, 2015.

[12] P. Gharghabi, J. Lee, M. S. Mazzola, and T. E. Lacy, "Development of an experimental setup to analyze carbon/epoxy composite subjected to current impulses," in *Proceedings of the American Society for Composites - 31st Technical Conference, ASC 2016*, 2016.

[13] P. K. Mallick, *Fiber-reinforced composites: Materials, manufacturing, and design*. Boca Raton: CRC Press, 2007.

[14] P. Duchene, S. Chaki, A. Ayadi, and P. Krawczak, "A review of non-destructive techniques used for mechanical damage assessment in polymer composites," *Journal of Materials Science*, vol. 53, no. 11, pp. 7915–7938, 2018.

[15] H. Towsyfyan, A. Biguri, R. Boardman, and T. Blumensath, "Successes and challenges in non-destructive testing of aircraft composite structures," *Chinese Journal of Aeronautics*, vol. 33, no. 3, pp. 771–791, 2020.

[16] S. Heimbs, S. Heller, P. Middendorf, F. Hähnel, and J. Weiße, "Low velocity impact on cfrp plates with compressive preload: Test and modelling," *International Journal of Impact Engineering*, vol. 36, no. 10–11, pp. 1182–1193, 2009.

[17] S. Heimbs, T. Bergmann, D. Schueler, and N. Toso-Pentecôte, "High velocity impact on preloaded composite plates," *Composite Structures*, vol. 111, no. 1, pp. 158–168, 2014.

[18] S. R. Doctor, T. E. Hall, and L. D. Reid, "Saft - the evolution of a signal processing technology for ultrasonic testing," *NDT International*, vol. 19, no. 3, pp. 163–167, 1986.

[19] A. Benammar, R. Drai, and A. Guessoum, "Detection of delamination defects in cfrp materials using ultrasonic signal processing," *Ultrasonics*, vol. 48, no. 8, pp. 731–738, 2008.

[20] S. S. Technologies, *Health monitoring of aerospace structures*. 2003.

[21] F. Honarvar, H. Sheikhzadeh, M. Moles, and A. N. Sinclair, "Improving the time-resolution and signal-to-noise ratio of ultrasonic nde signals," *Ultrasonics*, vol. 41, no. 9, pp. 755–763, 2004.

[22] E. Jasiūnienė, L. Mažeika, V. Samaitis, V. Cicėnas, and D. Mattsson, "Ultrasonic non-destructive testing of complex titanium/carbon fibre composite joints," *Ultrasonics*, vol. 95, pp. 13–21, 2019.

[23] P. Cawley and R. Adams, "Defect types and non-destructive testing techniques for composites and bonded joints. materials science and technology, 1989. 5(5): p. 413-425.," *Materials Science and Technology*, vol. 5, no. May, pp. 413–425, 1989.

[24] R. Ramzi, M. F. Mahmod, and E. A. Bakar, "Immersion ultrasonic inspection system for small scaled composite specimen," *ARPN Journal of Engineering and Applied Sciences*, vol. 10, no. 22, pp. 17146–17150, 2015.

[25] K. K. Borum, "Evaluation of the quality of thick fibre composites using immersion and air-coupled ultrasonic techniques," in *European conference on non-destructive testing*, German Society for Non-Destructive Testing, 2006.

[26] L. Gao, F. Zai, S. Su, H. Wang, P. Chen, and L. Liu, "Study and application of acoustic emission testing in fault diagnosis of low-speed heavy-duty gears," *Sensors*, vol. 11, no. 1, pp. 599–611, 2011.

[27] S. Gholizadeh, Z. Lemana, and B. T. H. T. Baharudin, "A review of the application of acoustic emission technique in engineering," *Structural Engineering and Mechanics*, vol. 54, no. 6, pp. 1075–1095, 2015.

[28] J. Arumugam, C. S. Kumar, C. Santulli, F. Sarasini, and A. J. Stanley, "A global method for the identification of failure modes in fiberglass using acoustic emission," *Journal of Testing and Evaluation*, vol. 39, no. 5, pp. 1–13, 2011.

[29] Y. H. Yu, J. H. Choi, J. H. Kweon, and D. H. Kim, "A study on the failure detection of composite materials using an acoustic emission," *Composite Structures*, vol. 75, no. 1–4, pp. 163–169, 2006.

[30] B. Wang, S. Zhong, T. L. Lee, K. S. Fancey, and J. Mi, "Non-destructive testing and evaluation of composite materials/structures: A state-of-the-art review," *Advances in Mechanical Engineering*, vol. 12, no. 4, pp. 1–28, 2020.

[31] A. Hase, H. Mishina, and M. Wada, "Correlation between features of acoustic emission signals and mechanical wear mechanisms," *Wear*, vol. 292–293, pp. 144–150, 2012.

[32] J. Y. Liu, P. F. Chu, J. K. Liu, and Y. L. Zheng, "A study on the failure mechanisms of carbon fiber/epoxy composite laminates using acoustic emission," *Materials & Design*, 2012.

[33] C. R. Ramirez-Jimenez, N. Papadakis, N. Reynolds, T. H. Gan, P. Purnell, and M. Pharaoh, "Identification of failure modes in glass/polypropylene composites by means of the primary frequency content of the acoustic emission event," *Composites Science and Technology*, vol. 64, no. 12, pp. 1819–1827, 2004.

[34] H. Towsyfyan, *Behaviour of mechanical seals for online condition monitoring.* PhD thesis, 2017.

[35] H. Nechad, A. Helmstetter, R. E. Guerjouma, and D. Sornette, "Creep ruptures in heterogeneous materials," *Physical Review Letters*, vol. 94, no. 4, pp. 1–4, 2005.

[36] H. Y. Chou, A. P. Mouritz, M. K. Bannister, and A. R. Bunsell, "Acoustic emission analysis of composite pressure vessels under constant and cyclic pressure," *Composites Part A: Applied Science and Manufacturing*, vol. 70, pp. 111–120, 2015.

[37] S. Huguet, N. Godin, R. Gaertner, L. Salmon, and D. Villard, "Use of acoustic emission to identify damage modes in glass fibre reinforced polyester," *Composites Science and Technology*, vol. 62, no. 10–11, pp. 1433–1444, 2002.

[38] N. Godin, S. Huguet, R. Gaertner, and L. Salmon, "Clustering of acoustic emission signals collected during tensile tests on unidirectional glass/polyester composite using supervised and unsupervised classifiers," *NDT & E International*, vol. 37, no. 4, pp. 253–264, 2004.

[39] E. Z. Kordatos, K. G. Dassios, D. G. Aggelis, and T. E. Matikas, "Rapid evaluation of the fatigue limit in composites using infrared lock-in thermography and acoustic emission," *Mechanics Research Communications*, vol. 54, pp. 14–20, 2013.

[40] B. Wang, S. Zhong, T. L. Lee, K. S. Fancey, and J. Mi, "Non-destructive testing and evaluation of composite materials/structures: A state-of-the-art review," *Advances in Mechanical Engineering*, vol. 12, no. 4, pp. 1–28, 2020.

[41] P. Vaara and J. Leinonen, "Technology survey on ndt of carbon-fiber composites," 2012.

[42] X. E. Gros, "Characterization of low energy impact damages in composites,"

[43] J. C. Moulder, E. Uzal, and J. H. Rose, "Thickness and conductivity of metallic layers from eddy current measurements," *Review of Scientific Instruments*, vol. 63, no. 6, pp. 3455–3465, 1992.

[44] P. Chandra and R. Bhagi, "Basics eddy current testing: Basics," 2014.

[45] G. Mook, R. Lange, and O. Koeser, "Non-destructive characterisation of carbon-fibre-reinforced plastics by means of eddy-currents," *Composites Science and Technology*, vol. 61, no. 6, pp. 865–873, 2001.

[46] J. Cheng, J. Qiu, H. Ji, E. Wang, T. Takagi, and T. Uchimoto, "Application of low frequency ect method in noncontact detection and visualization of cfrp material," *Composites Part B: Engineering*, vol. 110, pp. 141–152, 2017.

[47] G. Y. Tian and A. Sophian, "Reduction of lift-off effects for pulsed eddy current ndt," *NDT & E International*, vol. 38, no. 4, pp. 319–324, 2005.

[48] Y. Y. Hung and H. P. Ho, "Shearography: An optical measurement technique and applications," *Materials Science and Engineering: R: Reports*, vol. 49, no. 3, pp. 61–87, 2005.

[49] Q. Zhao, X. Dan, F. Sun, Y. Wang, S. Wu, and L. Yang, "Digital shearography for ndt: Phase measurement technique and recent developments," *Applied Sciences (Switzerland)*, vol. 8, no. 12, 2018.

[50] H. J. T. Pedrini, G., and Y. L. Zou, "Quantitative evaluation of digital shearing interferogram using the spatial carrier method." Pure and Applied Optics: Journal of the European Optical Society.

[51] M. K. Kalms, W. Osten, and W. P. O. Jueptner, "Advanced shearographic system for nondestructive testing of industrial and artwork components," in *Lasers in Material Processing and Manufacturing*, vol. 4915, p. 34, 2002.

[52] Y. Y. Hung, "Applications of digital shearography for testing of composite structures," *Composites Part B: Engineering*, vol. 30, no. 7, pp. 765–773, 1999.

[53] J. W. Newman, "Aerospace ndt with advanced laser shearography," in *17th World Conference on Nondestructive Testing*, pp. 25–28, 2008.

[54] Y. Y. Hung, W. D. Luo, L. Lin, and H. M. Shang, "Evaluating the soundness of bonding using shearography," *Composite Structures*, vol. 50, no. 4, pp. 353–362, 2000.

[55] J. R. Lee, J. Molimard, A. Vautrin, and Y. Surrel, "Application of grating shearography and speckle shearography to mechanical analysis of composite material," *Composites Part A: Applied Science and Manufacturing*, vol. 35, no. 7–8, pp. 965–976, 2004.

[56] F. Taillade, M. Quiertant, K. Benzarti, and C. Aubagnac, "Shearography and pulsed stimulated infrared thermography applied to a nondestructive evaluation of frp strengthening systems bonded on concrete structures," *Construction and Building Materials*, vol. 25, no. 2, pp. 568–574, 2011.

[57] "*dr. ip recently joined the mechanical engineering department of hong kong university.."

[58] G. D. Angelis, M. Meo, D. P. Almond, S. G. Pickering, and S. L. Angioni, "A new technique to detect defect size and depth in composite structures using digital shearography and unconstrained optimization," *NDT & E International*, vol. 45, no. 1, pp. 91–96, 2012.

[59] W. J. Murri *et al.*, "Defects in thick composites and some methods to locate them advanced methods group, physics division introduction nondestructive evaluation (nde) of thick composites is a difficult if ultrasonic techniques are used, such factors as attenuation (prefe)," 1991.

[60] Y. Y. Hung, L. X. Yang, and Y. H. Huang, *Non-destructive evaluation (NDE) of composites: Digital shearography.* No. 1, 2013.

[61] S. Gholizadeh, "A review of non-destructive testing methods of composite materials," *Procedia Structural Integrity*, vol. 1, pp. 50–57, 2016.

[62] J. Lee, F. Wu, W. Zhao, M. Ghaffari, L. Liao, and D. Siegel, "Prognostics and health management design for rotary machinery systems - reviews, methodology and applications," *Mechanical Systems and Signal Processing*, vol. 42, no. 1–2, pp. 314–334, 2014.

[63] H. O. Nyongesa, A. W. Otieno, and P. L. Rosin, "Neural fuzzy analysis of delaminated composites from shearography imaging," *Composite Structures*, vol. 54, no. 2–3, pp. 313–318, 2001.

[64] C. Meola, *Infrared thermography: Recent advances and future trends.* Sharjah, UAE: Bentham eBooks, 2012.

[65] Y. K. Zhu, G. Y. Tian, R. S. Lu, and H. Zhang, "A review of optical ndt technologies," *Sensors*, vol. 11, no. 8, pp. 7773–7798, 2011.

[66] S. Pickering and D. Almond, "Matched excitation energy comparison of the pulse and lock-in thermography nde techniques," *NDT & E International*, vol. 41, no. 7, pp. 501–509, 2008.

[67] R. Mulaveesala, G. Dua, and V. Arora, *Applications of infrared thermography for non-destructive characterization of concrete structures*, pp. 1–16. 2019.

[68] K. E. Cramer, "Current and future needs and research for composite materials nde," vol. 1059603, p. 500, 2018.

[69] A. ASTM, "Practice for infrared flash thermography of composite panels and repair patches used in aerospace applications. report no: E2582-07," 2007.

[70] F. Ciampa, P. Mahmoodi, F. Pinto, and M. Meo, "Recent advances in active infrared thermography for non-destructive testing of aerospace components," *Sensors (Switzerland)*, vol. 18, no. 2, 2018.

[71] F. Khodayar, F. Lopez, C. Ibarra-Castanedo, and X. Maldague, "Optimization of the inspection of large composite materials using robotized line scan thermography," *Journal of Nondestructive Evaluation*, vol. 36, no. 2, 2017.

[72] D. Bates, G. Smith, D. Lu, and J. Hewitt, "Rapid thermal non-destructive testing of aircraft components," *Composites Part B: Engineering*, vol. 31, no. 3, pp. 175–185, 2000.

[73] F. Khodayar, F. Lopez, C. Ibarra-Castanedo, and X. Maldague, "Parameter optimization of robotized line scan thermography for cfrp composite inspection," *Journal of Nondestructive Evaluation*, vol. 37, no. 1, 2018.

[74] B. Wiecek, "Review on thermal image processing for passive and active thermography," in *Annual International Conference of the IEEE Engineering in Medicine and Biology - Proceedings*, vol. 7 VOLS, pp. 686–689, 2005.

[75] S. Doshvarpassand, C. Wu, and X. Wang, "An overview of corrosion defect characterization using active infrared thermography," *Infrared Physics & Technology*, vol. 96, no. November 2018, pp. 366–389, 2019.

[76] P. Theodorakeas, E. Cheilakou, E. Ftikou, and M. Koui, "Passive and active infrared thermography: An overview of applications for the inspection of mosaic structures," *Journal of Physics: Conference Series*, vol. 655, no. 1, 2015.

[77] X. Maldague, *Theory and practice of infrared technology for nondestructive testing*. Hoboken: John Wiley & Sons, 2001.

[78] T. Zweschper, G. Riegert, A. Dillenz, and G. Busse, "Ultrasound excited thermography - advances due to frequency modulated elastic waves," *Quantitative Infrared Thermography Journal*, vol. 2, no. 1, pp. 65–76, 2005.

[79] B. Yang, Y. Huang, and L. Cheng, "Defect detection and evaluation of ultrasonic infrared thermography for aerospace cfrp composites," *Infrared Physics & Technology*, vol. 60, pp. 166–173, 2013.

[80] J. Wilson, G. Y. Tian, I. Z. Abidin, S. Yang, and D. Almond, "Modelling and evaluation of eddy current stimulated thermography," *Nondestructive Testing and Evaluation*, vol. 25, no. 3, pp. 205–218, 2010.

[81] T. J. Ahmed, G. F. Nino, H. E. N. Bersee, and A. Beukers, "Heat emitting layers for enhancing nde of composite structures," *Composites Part A: Applied Science and Manufacturing*, vol. 39, no. 6, pp. 1025–1036, 2008.

[82] C. Meola *et al.*, "Impact damaging of composites through online monitoring and non-destructive evaluation with infrared thermography," *NDT & E International*, vol. 85, pp. 34–42, 2017.

[83] M. Ishikawa and M. Koyama, "Influence of composite ply layup on active thermographic non-destructive inspection of carbon fiber-reinforced plastic laminates," *Journal of Nondestructive Evaluation*, vol. 37, no. 2, 2018.

[84] H. Towsyfyan, A. Biguri, R. Boardman, and T. Blumensath, "Successes and challenges in non-destructive testing of aircraft composite structures," *Chinese Journal of Aeronautics*, vol. 33, no. 3, pp. 771–791, 2020.

[85] C. Maierhofer, P. Myrach, M. Reischel, H. Steinfurth, M. Röllig, and M. Kunert, "Characterizing damage in cfrp structures using flash thermography in reflection and transmission configurations," *Composites Part B: Engineering*, vol. 57, pp. 35–46, 2014.

[86] D. P. Almond and W. Peng, "Thermal imaging of composites," *Journal of Microscopy*, vol. 201, no. 2, pp. 163–170, 2001.

[87] C. D. Lockard, "Anomaly detection in radiographic images of composite materials via crosshatch regression."

[88] H. Rolland, N. Saintier, P. Wilson, J. Merzeau, and G. Robert, "In situ x-ray tomography investigation on damage mechanisms in short glass fibre reinforced thermoplastics: Effects of fibre orientation and relative humidity," *Composites Part B: Engineering*, vol. 109, pp. 170–186, 2017.

[89] S. Gholizadeh, "A review of non-destructive testing methods of composite materials," *Procedia Structural Integrity*, vol. 1, pp. 50–57, 2016.

[90] S. Saber and G. I. Selim, "Higher-order statistics for automatic weld defect detection," *Journal of Software Engineering and Applications*, vol. 6, no. 5, pp. 251–258, 2013.

[91] F. J. Guild, N. Vrellos, B. W. Drinkwater, N. Balhi, S. L. Ogin, and P. A. Smith, "Intra-laminar cracking in cfrp laminates: Observations and modelling," *Journal of Materials Science*, vol. 41, no. 20, pp. 6599–6609, 2006.

[92] A. Ataş and C. Soutis, "Subcritical damage mechanisms of bolted joints in cfrp composite laminates," *Composites Part B: Engineering*, vol. 54, no. 1, pp. 20–27, 2013.